Evaluating the Arabian Sea as a regional source of atmospheric CO2: seasonal variability and drivers

Alain de Verneil, Zouhair Lachkar, Shafer Smith, Marina Lévy

https://doi.org/10.5194/bg-2021-22
Preprint. Discussion started: 17 February 2021

Biogeosciences Discussions
Open Access
EGU

Evaluating the Arabian Sea as a regional source of atmospheric CO_2: seasonal variability and drivers

Alain de Verneil[1], Zouhair Lachkar[1], Shafer Smith[2], and Marina Lévy[3]

[1]Center for Protoype Climate Modeling, New York University Abu Dhabi, Abu Dhabi, UAE
[2]Courant Institute of Mathematical Sciences, New York University, New York, USA
[3]Sorbonne Université (CNRS/IRD/MNHN), LOCEAN-IPSL, Paris, France

Correspondence: Alain de Verneil, (ajd11@nyu.edu)

Abstract. The Arabian Sea (AS) was confirmed to be a net emitter of CO_2 to the atmosphere during the international Joint Global Ocean Flux Study program of the 1990s, but since then little *in situ* data has been collected, leaving data-based methods to calculate air-sea exchange with fewer data and potentially out-of-date. Additionally, coarse-resolution models under-estimate CO_2 flux compared to other approaches. To address these shortcomings, we employ a high-resolution ($1/24^o$) regional model to quantify the seasonal cycle of air-sea CO_2 exchange in the AS by focusing on two main contributing factors, pCO_2 and winds. We compare the model to available *in situ* pCO_2 data and find that uncertainties in dissolved inorganic carbon (DIC) and total alkalinity (TA) lead to the greatest discrepancies. Nevertheless, the model is more successful than neural network approaches in replicating the large variability in summertime pCO_2 because it captures the AS's intense monsoon dynamics. In the seasonal pCO_2 cycle, temperature plays the major role in determining surface pCO_2, except where DIC delivery is important in summer upwelling areas. Since seasonal temperature forcing is relatively uniform, pCO_2 differences between the AS's sub-regions are mostly caused by geographic DIC gradients. We find that primary productivity during both summer and winter monsoon blooms, but also generally, is insufficient to off-set the physical delivery of DIC to the surface, resulting in limited biological control of CO_2 release. The most intense air-sea CO_2 exchange occurs during the summer monsoon where outgassing rates reach $\sim\mathbf{6\ molCm^{-2}yr^{-1}}$ in the upwelling regions of Oman and Somalia, but the entire AS contributes CO_2 to the atmosphere. Despite a regional spring maximum of pCO_2 driven by surface heating, CO_2 exchange rates peak in summer due to winds, which account for $\sim$**90%** of the summer CO_2 flux variability versus **6%** for pCO_2 in a Reynolds decomposition. In comparison with other estimates, we find that the AS emits $\sim\mathbf{160TgCyr^{-1}}$, slightly higher than previously reported. Altogether, there is **2x** variability in annual flux magnitude across methodologies considered. Future attempts to reduce the variability in estimates will likely require more *in situ* carbon data. Since summer monsoon winds are critical in determining flux both directly and indirectly through temperature, DIC, TA, mixing, and primary production effects on pCO_2, studies looking to predict CO_2 emissions in the AS with ongoing climate change will need to correctly resolve their timing, strength, and upwelling dynamics.

https://doi.org/10.5194/bg-2021-22
Preprint. Discussion started: 17 February 2021

Biogeosciences Discussions Open Access EGU

1 Introduction

The global ocean represents a major reservoir of inorganic carbon on the planet's surface, and up to the present has on average acted to uptake excess anthropogenic CO_2 (Ciais et al., 2013; Khatiwala et al., 2009). The Arabian Sea (AS) is a region of the ocean that has been found to naturally release CO_2 to the atmosphere (Sarma et al., 1998), mitigating the ocean's role in moderating atmospheric CO_2 accumulation. While the AS as a regional basin is considered too small to greatly impact global budgets of air-sea CO_2 exchange (Naqvi et al., 2005), it attracts attention because some of the highest rates of air-sea CO_2 flux and values of partial pressure of CO_2, or pCO_2, have been observed there, in addition to unique features such as the world's thickest oxygen minimum zone (OMZ) (Lachkar et al., 2016) and corresponding Carbon Maximum Zone (CMZ) (Paulmier et al., 2011).

The role of the AS as a region of net CO_2 emission, while suspected for decades (Keeling, 1968; Naqvi et al., 1993), was more firmly established with observations conducted under the international collaborative efforts of the Joint Global Ocean Flux Study (JGOFS) program during the 1990s (Sarma et al., 1998; Millero et al., 1998a; Goyet et al., 1998b; Naqvi et al., 2005); see Smith (2005) and the accompanying Progress in Oceanography special issue for greater context. Conducted over several years, a major focus was to sample over the particularly strong seasonal monsoon cycle present in the AS, complete with surface current reversals, coastal upwelling, and intense phytoplankton blooms (Schott and McCreary Jr, 2001; Kumar et al., 2001; Lévy et al., 2007). JGOFS carbon data were first used to create linear statistical models, which were then extrapolated over a greater region of the AS to produce larger-scale estimates of seasonal CO_2 flux showing emission to the atmosphere (Sabine et al., 2000; Sarma, 2003; Bates et al., 2006). JGOFS data still represent the greatest source of data for current de facto standard global products, such as Takahashi et al. (2009) (hereafter TK09), who produced a global climatology of pCO_2 and CO_2 flux gridded onto a 4^o x 5^o grid using a horizontal advection-diffusion scheme. In recent years, neural networks have been applied instead of simpler statistical models to likewise produce global climatologies, such as Landschützer et al. (2015) (hereafter L15) on an increased-resolution 1^o x 1^o grid. All these different methodologies, although of differing sophistication, still rely on the availability of *in situ* data.

The wealth of information provided by the JGOFS expeditions has been invaluable for understanding the AS, but there has been little subsequent *in situ* sampling in the AS, as has been previously remarked (Hood et al., 2016). For example, in the Global Ocean Data Analysis Project v2 (GLODAP; Olsen et al., 2019) database, there are no reported observations in the AS of two important carbon variables, dissolved inorganic carbon (DIC) and total alkalinity (TA), more recent than 1998, with a similar story for pCO_2. Thus, the global products of TK09 and L15 are based upon conditions in the AS from 20 years ago. Since quantities like surface pCO_2 concurrently trend with rising atmospheric CO_2 concentration (Tjiputra et al., 2014), the dearth of recent sampling means that uncertainty in the AS's carbon system will only grow with time. The gap in data collection also means that the AS is proportionally under-represented in global datasets: whereas the AS is 2% of the ocean surface, DIC and TA measurements in the AS are <1% of the GLODAP ensemble, which is also the case with pCO_2 reported in the Surface Ocean Carbon ATlas (SOCAT; Bakker et al., 2016; Pfeil et al., 2013).

https://doi.org/10.5194/bg-2021-22
Preprint. Discussion started: 17 February 2021

Where data are sparse in the AS, numerical circulation models have been used to complement the lack of spatiotemporal coverage. These models fill the domain with their own estimates of carbon variables, such as pCO_2, while also providing detailed information on the factors affecting them, e.g. DIC, temperature, biological productivity, etc. For example, in the wake of the JGOFS expeditions, the synthesis study of Sarma et al. (2003) used a numerical model to examine biological and chemical aspects of the annual carbon budget in the central and eastern AS. Further studies focus on other aspects over different timescales, such as intraseasonal pCO_2 variability due to temperature versus DIC (Valsala and Murtugudde, 2015), or decadal trends in pH (Sreeush et al., 2019a). These approaches, without more *in situ* data, are the best estimates we have of the current AS carbon system's behavior. Therefore, it is incumbent that these models are vigorously validated against what precious few data exist. The need is further emphasized when quantities such as pCO_2 can be utilized as a proxy for other things, such as community compensation depth (Sreeush et al., 2019b). However, most recent studies compare output to established climatologies, such as TK09, which are coarse in spatial resolution and smooth out unique features of the AS such as coastal upwelling, although some studies have begun using ARGO float profiles for model validation (Chakraborty et al., 2018).

Despite the wealth of information that models provide, they have their own weaknesses. In a review of CO_2 flux estimates from various independent methodologies, Sarma et al. (2013) found that coupled ocean biogeochemical models underestimated the air-sea CO_2 flux. The underestimate was attributed to poor resolution of monsoonal currents, specifically near the coasts of Oman and Somalia. The need for sufficient resolution of monsoon and upwelling currents is underscored by the roles that small-scale horizontal (Mahadevan et al., 2004) and vertical (Mahadevan et al., 2011; Resplandy et al., 2019) currents can play in advecting carbon. Additionally, Sarma et al. (2013) found that the peak of flux observed in boreal summer occurred slightly out of phase, with models leading observations by over a month in the AS. Finally, the modeled pCO_2 in the AS found a springtime maximum not seen in the observations based on the data from TK09. Clearly, an effort must be made to establish whether these discrepancies are residual effects of low resolution, endemic to models generally, or indicative of a real pattern that suggests future concerted *in situ* sampling.

Considering the challenges specific to studying the AS carbon cycle, in this paper we aim to put into context the role of the AS as a CO_2 source by quantifying air-sea CO_2 flux with a targeted approach. First, by employing a higher-resolution regional numerical model of the AS carbon system, monsoonal and upwelling currents will be sufficiently resolved. Furthermore, model validation will use raw data, not a smoothed climatological product, to evaluate the model. Quantification of air-sea flux will focus on the contributing factors of pCO_2 and wind. In particular, the role of temperature (T), salinity (S), DIC, and TA in determining the seasonal cycle of pCO_2 will be investigated, which of course also varies from region to region within the AS. A further budget analysis of surface DIC compares the physical and biological mechanisms governing carbon sources and sinks, such as advection and mixing versus biological production and respiration. The relative impact of pCO_2 and winds upon the seasonal cycle of CO_2 flux are also compared, culminating in a meta-analysis of the model's CO_2 flux estimates relative to alternative approaches.

For this study, we choose to focus on the seasonal cycle due to the strength of the monsoon in the AS and because it is resolved by the data, although interannual (Valsala and Maksyutov, 2013; Valsala et al., 2020) and intraseasonal (Valsala and

https://doi.org/10.5194/bg-2021-22
Preprint. Discussion started: 17 February 2021

Murtugudde, 2015) variability exists. The rest of the paper will start with a description of pCO_2 datasets used, along with the model configuration and methods of analysis in Section 2. Following this in Section 3 is a description of the model validation and results, with discussion in Section 4. We conclude in Section 5 with perspectives and recommendations regarding future studies of pCO_2 and air-sea CO_2 flux in the AS.

2 Methods

2.1 pCO_2 data

In this study, pCO_2 is used as the primary *in situ* data for model validation. Whereas models favor DIC and TA (Wolf-Gladrow et al., 2007), shipboard pCO_2 can be measured underway and hence there are more observations available. Additionally, since model pCO_2 is calculated from DIC and TA, pCO_2 measurements act as an independent dataset. Here, pCO_2 validation stems from *in situ* un-gridded data merged from SOCAT v. 2019 (downloaded from https://www.socat.info/index.php/version-2019/ September 2019) and the Lamont-Doherty Earth Observatory (LDEO) surface pCO_2 database (Takahashi et al., 2019). Due to the large overlap in the two databases, SOCAT data was preferred to LDEO observations, and LDEO observations were included for years where SOCAT data are unreported. SOCAT fugacity (fCO_2) values were converted to pCO_2 and mole fraction (xCO_2) using reported sea surface temperature (SST) and S data included in the products. The anthropogenic effect of increasing surface pCO_2 was calculated by removing a fit linear trend of 2 $\mu\mathrm{atm\ yr}^{-1}$, slightly higher than ≈1.5 seen in Tjiputra et al. (2014). pCO_2 values were calibrated to the year 2005, the representative year used for the model's atmospheric xCO_2.

Alternative pCO_2 products are used for comparison purposes. The gridded products from TK09 and L15, while based upon the same *in situ* data mentioned above, represent different processing methodologies. pCO_2 is also calculated from DIC and TA provided by the statistical fits to JGOFS data by Sarma (2003) and to the gridded GLODAP climatological product. The statistical fits of Sarma (2003) were used twice, first using model T,S, and Chl-*a*, and second with World Ocean Atlas (WOA) 2009 T, S with SeaWifs Chl-*a*. GLODAP-derived pCO_2 also uses WOA2009 T, S. Calculations of pCO_2 are performed using the CO2SYS software package (Van Heuven et al., 2011). Since all calculations are conducted at the near-surface, differences between this software suite and Orr and Epitalon (2015) are minimal. For air-sea flux calculations, all ΔpCO_2 values were calculated using Keeling curve values (downloaded from https://www.esrl.noaa.gov/gmd/ccgg/trends/gl_data.html, downloaded September 2019) of atmospheric xCO_2 for the respective calibrated year of each data set (1995 for Sarma (2003), 2001 for L15, 2002 for GLODAP, 2005 for TK09). A summary of these datasets and their characteristics is provided in Table 1.

2.2 Model details and set-up

The model we use is the Regional Ocean Modeling System-AGRIF (ROMS-AGRIF) 3.1.1. Shchepetkin and McWilliams (2005). Previously used in the region (Lachkar et al., 2016), the model is a free-surface primitive equation model, with a sigma

https://doi.org/10.5194/bg-2021-22
Preprint. Discussion started: 17 February 2021

and curvilinear grid for the vertical and horizontal dimensions, respectively. ROMS implements a forward-backward time-stepping alogrithm with split baroclinic and barotropic modes. The advection of tracers implements a rotated-split 3rd order upstream biased algorithm for the advection of tracers to reduce spurious mixing (Marchesiello et al., 2009). The K-profile parameterization (KPP; Large et al., 1994) for vertical mixing is used. The model domain spans from 5.3^{o}S to 30.5^{o}N, and from 33^o to 78.1^{o}E (Fig. 1). For the sake of comparison with previous studies, we will present the region north of the equator, and exclude the Red Sea and Arabian Gulf. The model's horizontal resolution is 1/24^o, resulting in $\sim$5km horizontal grid spacing.

Coupled to the hydrodynamic model is a nitrogen-based biogeochemical model with two components for nutrients, nitrate and ammonium, with one phytoplankton, zooplankton, and two detrital pools (Gruber et al., 2006). Biological parameters for the model are the same as those used in Gruber et al. (2011). A carbon module is also applied to the model with the state variables of DIC, TA, and calcium carbonate ($CaCO_3$) (Gruber et al., 2012; Hauri et al., 2013; Lachkar and Gruber, 2013). In addition to usual physical transport and mixing, $CaCO_3$ is allowed to vertically sink at 20 mday^{-1}. Organic carbon is linked to organic nitrogen through the Redfield ratio 106:16. DIC is altered by air-sea CO_2 flux, primary production, respiration/remineralization, and dissolution/precipitation of $CaCO_3$. TA changes with the removal and creation of nitrate (NO_3) as well as dissolution/precipitation of $CaCO_3$. The amount of $CaCO_3$ precipitation is linked to primary production through a constant ratio of 0.07, meaning 0.07 moles of $CaCO_3$ are produced for each mole of organic carbon. The dissolution rate is a constant 0.0057 day^{-1} in the water column and 0.002 day^{-1} in the sediments. Surface fluxes of DIC and TA due to evaporation and precipitation were included as virtual fluxes. Inside the module, surface carbon chemistry is calculated using routines from the Ocean Carbon-Cycle Model Intercomparison Project (OCMIP) carbonate chemistry routines (http://ocmip5.ipsl.jussieu.fr/OCMIP/phase3/simulations/). Carbon chemistry coefficients used here include K_1 and K_2 CO_2 dissociation from Millero (1995), original data from Mehrbach et al. (1973) and refit by Dickson and Millero (1987).

The model was run in climatological mode, with 360-day years and interpolated monthly forcing. Heat flux, evaporation and precipitation, and surface salinity were provided by the Comprehensive Ocean-Atmosphere Data Set (COADS; da Silva et al., 1994). SST forcing is provided by a monthly climatology of Pathfinder data from 1985-1997 (Casey and Cornillon, 1999). Wind stress was produced using the QuikSCAT/SCOW monthly climatology from 1999-2009 (Risien and Chelton, 2008). Tracer values for the initial conditions and the boundaries are given by WOA 2009 for T, S, NO_3, and oxygen. Horizontal velocities u,v for initial and boundary conditions derive from the Simple Ocean Data Assimilation (SODA) analysis (Carton and Giese, 2008). Initial and boundary conditions for DIC and TA come from GLODAP from 300m down to the bottom. Surface TA was calculated using the relations from Lee et al. (2006), and the corresponding DIC was calculated using WOA phosphate, silicate, T, and S values along with L15 pCO_2. DIC and TA values between the surface and 300m were calculated using density-weighting. The model was spun up for 30 years, with 5 additional years for analysis. Atmospheric xCO_2 values are set to 380ppm, equivalent to 2005 levels, with an annual sinusoidal perturbation of 2.9ppm.

https://doi.org/10.5194/bg-2021-22
Preprint. Discussion started: 17 February 2021

2.3 Domains of Analysis

In this study we focus on 6 distinct regions (Fig. 1). The first, the entire analysis domain, is the AS north of the equator. The upwelling regions of the Oman and Somalian coasts are included separately to focus on the summer monsoon impact of enhanced DIC but also enhanced biological productivity. The Oman region begins at the coast and extends 300km outward. The Somalia region begins near 3.8^{o}N and extends north to the tip of the Horn of Africa, with an eastern extension to 58.6^{o}E so as to encompass the region known as the Great Whirl (Vic et al., 2014), shown to be important for air-sea exchange in previous studies (Valsala and Murtugudde, 2015). The North region is defined by a rectangle from 59.4^{o}E, 21^{o}N to 69.5^{o}E, 26.5^{o}N, encompassing the northern part of the AS where the winter monsoon's primary productivity is most intense. An oligotrophic region representing the central AS, which has less productivity and chlorophyll-a on average (Fig. 1), is defined by a rectangle from 61.31^{o}E, 3.3^{o}N to 70.8^{o}E, 17^{o}N. The last region, covering the western coast of India, extends from the coastline 100km offshore.

2.4 Analysis of pCO_2, DIC, and air-sea CO_2 flux variability

2.4.1 pCO_2 variability

The proximate variables impacting pCO_2 in the model are DIC, TA, T, and S. Following previous studies (Lovenduski et al., 2007; Turi et al., 2014), we use a first-order Taylor expansion to decompose pCO_2 into contributions from these four, neglecting contributions from nutrients (phosphate and silicate). Initially, the decomposition would follow the form

$$\Delta pCO_2 \approx \frac{\partial pCO_2}{\partial DIC}\Delta DIC + \frac{\partial pCO_2}{\partial TA}\Delta TA + \frac{\partial pCO_2}{\partial T}\Delta T + \frac{\partial pCO_2}{\partial S}\Delta S \tag{1}$$

where ΔpCO_2 is the perturbation of pCO_2 from a mean value, and the Δ terms for DIC, TA, T, and S likewise express deviations from an average. However, in order to control for salinity effects on DIC and TA (Keeling et al., 2004), we normalize DIC and TA by the salinity S_0=35 psu, to create the variables

$$DIC^s = S_0\frac{DIC}{S} \;\; and \;\; TA^s = S_0\frac{TA}{S}. \tag{2}$$

Substituting these terms into Eqn. (1), we can expand to produce, for example with DIC, the following (Lovenduski et al., 2007):

$$\begin{aligned}\frac{\partial pCO_2}{\partial DIC}\Delta DIC &= \frac{\partial pCO_2}{\partial (S/S_0 DIC^s)}\Delta(S/S_0 DIC^s) \\ &= \frac{DIC^s}{S_0}\frac{\partial pCO_2}{\partial DIC}\Delta S + \frac{S}{S_0}\frac{pCO_2}{\partial DIC}\Delta DIC^s.\end{aligned} \tag{3}$$

Collectively, the ΔS term in Eqn. (3) and its counterpart in TA can be added to the original ΔS term in Eqn. (1) to represent all salinity effects in a "freshwater" term, FW, so that we now have (Turi et al., 2014)

$$\Delta pCO_2 \approx \underbrace{\frac{\partial pCO_2}{\partial DIC^S}\Delta DIC^S}_{\Delta pCO_2^{DIC^s}} + \underbrace{\frac{\partial pCO_2}{\partial TA^S}\Delta TA^S}_{\Delta pCO_2^{TA^s}} + \underbrace{\frac{\partial pCO_2}{\partial T}\Delta T}_{\Delta pCO_2^{T}} + \underbrace{\frac{\partial pCO_2}{\partial FW}\Delta FW}_{\Delta pCO_2^{FW}}. \tag{4}$$

https://doi.org/10.5194/bg-2021-22
Preprint. Discussion started: 17 February 2021

For the remainder of this paper, when discussing the results of the Taylor series decomposition method, it will be understood that DIC and TA refer to DIC^s and TA^s.

The contributions of DIC, TA, T, and S to pCO_2 variability are used to construct maps and timeseries of pCO_2 anomalies. In order to calculate the anomaly ΔpCO_2 requires calculating both the Δ deviations of DIC, TA, T, and FW, as well as partial derivatives. In this study, we calculate both temporal and spatial anomalies. To consider spatial variability, starting with annual means of pCO_2, DIC, TA, T, and S, an average value for the whole domain is calculated and removed from each grid point's annual mean to get a Δ perturbation, or anomaly. Similarly, for temporal variability, with the monthly values of pCO_2, DIC, TA, T, and S at each grid point, the annual average at that grid point is removed to produce the monthly Δ perturbation/anomaly. Partial derivatives are approximated via centered differences. These are obtained by calculating pCO_2 with slight deviations of DIC, TA, T, and S from the mean value. Both positive and negative deviations are used to construct centered differences, with deviation magnitude determined by Orr et al. (2018).

2.4.2 DIC budget

Whereas the state variables of DIC, TA, T, and S provide the chemical context which determines carbon availability to potential air-sea flux via pCO_2, tracking the overall inventory of inorganic carbon (i.e. DIC), allows for the parsing of numerous source and sink processes governing the total amount of carbon reaching the surface. Beyond the biological processes impacting DIC as outlined in Sect. 2.2, the physical processes impacting DIC are air-sea CO_2 flux, surface evaporation and precipitation, horizontal and vertical advection, and horizontal and vertical mixing. In order to diagnose the relative importance of these terms (i.e. to weigh competition between upwelling circulation-source and biological drawdown-sink), we calculate the budget I_{DIC} in a 3D volume by integrating:

$$I_{DIC} = \iint_{\mathbf{A}} \int_{-z(\sigma)}^{\eta} J(x,y,z)\, d\mathbf{A}\, dz \tag{5}$$

with

$$J = \underbrace{-PP_{New+Reg} - CaCO_{3prec-remin} + Zoo_{resp} + Det_{remin}}_{NPP-Remin\ (Biology)} - \underbrace{F_{AS}}_{Air-Sea}$$
$$+ \underbrace{Adv_x + Adv_y + Mix_x + Mix_y}_{Horz.\ Circ} + \underbrace{Adv_z + Mix_z}_{Vert.\ Circ} + \underbrace{Evap - Precip}_{Forc}, \tag{6}$$

which is the volume-specific flux J of DIC in a given grid cell. $PP_{New+Reg}$ is net community primary production scaled by the Redfield ratio, $CaCO_{3remin-prec}$ is net $CaCO_3$ precipitation and remineralization, Zoo_{resp} is zooplankton respiration, and Det_{remin} is remineralization of both detrital pools. All these terms are grouped together into $NPP - Remin$ because they represent all biological processes. F_{AS} is air-sea flux, with a sign convention of positive outward. Adv_x is advective flux in the x-direction, with corresponding y and z components. Mix_x is the x-component of mixing flux, again with y and z components. All x and y components of both advective and mixing DIC fluxes are grouped into horizontal circulation, with a similar grouping for vertical circulation in the z-direction. $Evap - Precip$ is the forced virtual flux from evaporation and

https://doi.org/10.5194/bg-2021-22
Preprint. Discussion started: 17 February 2021

precipitation at the surface. **A** is the two-dimensional horizontal area to be considered, which in our study includes the entire domain but also the sub-regions of analysis. The bottom boundary of integration, $-z(\sigma)$, is the sigma-layer depth at which integration starts, moving up to the free-moving surface η. We chose to integrate the top five sigma layers of the model, corresponding to $\sim$20m depth. This level was chosen because below this depth, annual cycles of I_{DIC} begin to deviate from the surface DIC, which is our focus in this study of air-sea CO_2 flux.

2.4.3 Air-sea CO_2 variability

The air-sea flux in the model is calculated using

$$\begin{aligned} F_{CO_2} &= K_0\,\alpha\,(pCO_2^{sea} - pCO_2^{air}) \\ &= K_0\,\alpha\,\Delta pCO_2 \end{aligned} \tag{7}$$

where K_0 is the solubility determined by temperature and salinity (Weiss, 1974), α is the CO_2 piston velocity with a quadratic wind speed dependence (Wanninkhof, 1992), and the difference in ocean and atmosphere pCO_2, ΔpCO_2, is arranged so that the flux convention is positive outward from the ocean. The objective being to characterize seasonal anomalies of air-sea CO_2 flux, here we use a Reynolds decomposition (Doney et al., 2009). Noting that temperature effects upon solubility (K_0) and piston velocity (α) approximately cancel, meaning that their product mostly reflects wind forcing, we have the following arrangement for the decomposition of flux anomalies (see Doney et al. (2009) for the derivation):

$$F'_{CO_2} = \underbrace{(K_0\,\alpha)'\overline{\Delta pCO_2}}_{\text{wind}} + \underbrace{\overline{(K_0\,\alpha)}\Delta pCO'_2}_{\text{pCO}_2} + \underbrace{\Big((K_0\,\alpha)'(\Delta pCO_2)' - \overline{(K_0\,\alpha)'\Delta pCO'_2}\Big)}_{\text{cross terms}}, \tag{8}$$

where $'$ indicates an anomaly and $\overline{x}$ is a five-year average of variable x, which are calculated at each grid point. F'_{CO_2} is the seasonal flux anomaly, with groupings based on wind anomalies $(K_0\,\alpha)'$, $\Delta pCO'_2$ anomalies, and cross-terms involving both.

3 Results

3.1 Model validation and pCO_2 data-model comparisons

The implementation of ROMS-AGRIF presented here has been used in previous studies (Lachkar et al., 2016). Model output of net primary productivity (NPP) captures the summer monsoon highs near the upwelling regions of Oman and Somalia, with enhanced NPP in the North during the winter monsoon (Fig. 1). The model also reproduces well the distribution of temperature, salinity, and surface velocities in comparison with established climatologies (Fig. S1-S3).

Regarding pCO_2, *in situ* data from the merged SOCAT/LDEO database shows that average binned ΔpCO_2 values in the region are positive for most of the AS (Fig. 2a). The ensemble of observations show that $\sim$90% of ΔpCO_2 observations are positive, indicating positive flux to the atmosphere (Fig. 2a, inset). The monthly distribution of pCO_2 sampling (Fig. 2b) also shows that the majority of data ($\sim$70%) come from the summer monsoon months (June-September JJAS), and that most observations date from the 1990s, with 96% coming from the years 1995 and 1997 alone.

https://doi.org/10.5194/bg-2021-22
Preprint. Discussion started: 17 February 2021

Seasonal pCO_2 distributions from both data and the model are shown in Fig. 3. During the winter monsoon, pCO_2 values are at their lowest (348-455 μatm; Fig. 3a). Spring intermonsoon (Fig. 3b) finds pCO_2 values similar to the winter (354-451 μatm), with data coverage improving in the western AS. Summer monsoon, with best data coverage (Fig. 3c), has pCO_2 peaking at 773 μatm. In contrast, the fall intermonsoon (Fig. 3d) has very little data coverage (311-485 μatm). Similar to the data, model pCO_2 (Fig. 3e) is at its lowest during the winter, but in the spring, open-ocean pCO_2 finds its peak, which is not reflected in the *in situ* data set (Fig. 3b,f). Maximum model pCO_2 is found in the summer monsoon near upwelling reigons (Fig. 3g). Fall model pCO_2 still has elevated values, but less than the summer period. Certain regions in the model show persistent maxima in pCO_2, such as the Gulf of Oman and the Strait of Hormuz, which are not reflected in the few data collected there. Similarly, model pCO_2 values in the Gulf of Aden increase during spring and then peak during the summer, a pattern which is unclear from the data.

A Taylor diagram (Taylor, 2001) comparing *in situ* pCO_2 data and model output shows the relative performance of the model (Fig. 4). For the entire dataset, as well as for the spring and summer seasons, the model's correlation with data is $\sim$0.5. Winter and fall have lower values at 0.2 and 0.06, respectively. Variability expressed as normalized standard deviation shows that overall, and during spring and summer periods, the model under-estimates data variability, but over-estimates it during winter and fall. For all periods apart from summer, model pCO_2 has a positive bias (2.1, 24.6, 48.4, and 33.7 μatm for the annual, winter, spring, and fall seasons, respectively). During the summer, the model has a negative bias of -3.1 μatm.

Since the model successfully replicates other tracers, physics, and biological processes (Fig. 1, Fig. S1-S3), we look for the source of bias within the four state variables T, S, DIC, and TA in comparison with data. T and S from the merged LDEO/SOCAT database, and DIC, TA, from the ungridded GLODAP product are compared with model output (Fig. S4). In this case, model SST and surface salinity (Fig. S4a,b) largely overlap with a 1:1 relationship, but with slight positive biases of $\approx 0.4^{o}C$ and $0.3 psu$. Removing these biases from the model results in a pCO_2 shift of -6.8 and -3.5 μatm for T and S, respectively, close to reported measurement error. Ungridded DIC and TA data from GLODAP, though more sparse (n=334 data points with both DIC and TA at depth $\leq 50m$), show more deviation from the 1:1 line (Fig. S4c,d) with overall negative biases of -15.8 $\mu mol kg^{-1}$ and -30.0 $\mu mol - eq kg^{-1}$ for DIC and TA. These biases result in pCO_2 perturbations of -33.8 and +45.7 μatm, respectively, when accounted for individually. Since the buffering capacity of seawater is related to the ratio of TA and DIC, when both biases are considered average pCO_2 shifts +16.7 μatm. As a result, while the DIC model bias lowers pCO_2, the stronger bias in TA is the most likely cause for the model's overall positive pCO_2 bias.

Comparisons between the monthly probability distribution functions of pCO_2 from *in situ* data, model output, and L15 demonstrate temporal variability between pCO_2 products (Fig. 5). For most of the year, the data (Fig. 5a) stays within a relatively narrow range (375-425 μatm), except for the summer monsoon where values can exceed 500 μatm and the median value has its peak. In the model (Fig. 5b), pCO_2 is almost entirely above 400 μatm, with the median value increasing during spring inter-monsoon and peaking in June. Similar to the data, the upper bound variability in pCO_2 peaks in August. L15 (Fig. 5c), by contrast, has a tighter envelope of variability, with 5-95 percentile values never going beyond the range of 368-434 μatm. Median pCO_2 in L15 peaks in the summer like the data, but there is no large increase in upper bound variability.

https://doi.org/10.5194/bg-2021-22
Preprint. Discussion started: 17 February 2021

In summary, the survey of available data and comparing it to the model output produces a few distinct features: 1) available *in situ* data shows that the majority of observations are skewed towards the summer monsoon during the years 1995 and 1997; 2) most *in situ* data show CO_2 out-gassing in the AS; 3) the model has a net positive bias in surface pCO_2, driven by a joint DIC-TA bias which is slightly stronger in TA; and 4) the model captures the high summer monsoon pCO_2 values better than competing products.

3.2 pCO_2 distribution, seasonal cycle, and underlying contributors

3.2.1 Spatial pCO_2 distribution

Spatial pCO_2 anomalies from the regional mean highlight the geographic hotspots of pCO_2 inside the domain (Fig 6a). Within the regions of analysis prescribed in this study, it is clear that Oman, the Indian coast, and the North AS including the Gulf of Oman host enhanced pCO_2. In contrast, both the oligotrophic central AS and Somalia regions have negative pCO_2 anomalies. The contributing factors to these pCO_2 anomalies, temperature, DIC, TA, and freshwater components, display differing distributions. Temperature (Fig. 6c) contributes toward negative pCO_2 anomalies in a southwest-to-northeast band along the coasts of east Africa and the Arabian peninsula, up to the coasts of Pakistan and northern coast of India near Gujarat. The cold SST structure largely overlaps the stronger summer monsoon winds. The opposite trend is found in the central oligotrophic and Indian regions, where temperature contributes positively to pCO_2 anomaly, despite upwelling in the southern Indian coast. The distribution of DIC-induced anomalies (Fig. 6d) shows a positive influence near coastal regions and the western AS off the coast of Somalia, whereas a strong minimum is found in an oval region encompassing the central, open-ocean AS. TA effects (Fig. 6e) show a north-south gradient with positive contributions to pCO_2 occurring in the north and negative towards the south, in a similar distribution to surface salinity gradients in the AS. Freshwater contributions (Fig. 6f) show a similar distribution as TA, but weaker in magnitude for all regions.

Putting together all the spatial anomalies for each region, different variables become dominant (Fig. 6b). Near Oman, temperature is a strong negative factor, but it is counteracted mostly by DIC and the other effects to produce a positive anomaly. A similar pattern occurs for the North, but in this case TA and freshwater effects play a larger role than DIC. In the oligotrophic region, the strong negative DIC effect swamps all other effects. In the Somalia upwelling region, the strong positive DIC influence is stronger than opposing temperature, but TA and freshwater effects are enough to produce a slightly negative pCO_2 anomaly. The coast of India, influenced most likely by its shelf, has a very high positive DIC contribution, more than enough to overrule other variables.

3.2.2 Seasonal pCO_2 cycle

The previous section outlines why certain geographic regions within the AS have overall high or low pCO_2 values, but in order to investigate the strong seasonal monsoon impact in the AS, the decomposition of factors affecting monthly pCO_2 values is calculated at each model grid point and averaged into each analysis region (Fig. 7). Regarding the whole domain (Fig. 7a), pCO_2 variability is similar to that seen in Fig. 5b, with a spring pCO_2 peak and minimum during fall and winter. Temperature

https://doi.org/10.5194/bg-2021-22
Preprint. Discussion started: 17 February 2021

effects largely mirror the overall pCO_2 cycle. DIC acts in opposition to temperature but with lower magnitude. Both TA and freshwater effects are negative for the first half of the year before becoming slightly positive in the second half. The oligotrophic central region (Fig. 7d), the largest in area, has similar pCO_2 and temperature impacts as the whole domain, with the two largely overlapping. DIC, TA, and freshwater impacts also follow similar patterns, but have slightly higher magnitudes in the central AS.

Different pCO_2 anomaly cycles can be found in the upwelling regions of Oman, Somalia and India (Fig. 7b,e,f). Here, a positive temperature peak appears in the spring, which is then supplanted by a positive DIC peak during the summer monsoon. In both Oman and India, the summertime DIC peak is strong enough to contribute to the annual pCO_2 peak despite cooler temperatures. In Somalia, the summertime DIC peak is not sufficiently stronger than temperature, and the maximum pCO_2 is found in the spring like in the whole domain and oligotrophic regions. Both TA and freshwater effects in these three regions are lower in magnitude and generally run counter to DIC.

A completely different regime occurs in the North AS (Fig. 7c). Here, while temperature effects create a similar spring-summertime peak in pCO_2 somewhat counter-acted by DIC, during the winter monsoon temperature and DIC effects are both maximal and in opposing amplitudes. This occurs due to the convective mixing that occurs during winter in the North AS, where cooling temperatures lower pCO_2 but subsurface water introduces more DIC, resulting in a near-balance.

The spatial and seasonal decomposition of pCO_2 anomalies in the AS demonstrate how the four variables of DIC, TA, T, and freshwater differently impact sub-regions in the AS, on the whole and within seasons. The upwelling and coastal regions show elevated pCO_2 relative to the whole AS, which is due to enhanced DIC and counter-acted by lower temperatures. The central, oligotrophic AS has lower relative pCO_2 due to a strong negative DIC anomaly. Analyzing the seasonal cycle within the domain and its sub-regions, temperature anomalies are most responsible for pCO_2 variability, generally peaking in the spring. Positive DIC contributions to seasonal pCO_2 anomalies become important in the upwelling zones during the summer monsoon, as well as the North AS due to wintertime convective mixing.

3.3 Near-surface DIC budgets and cycling

Whereas SST and its effect on pCO_2 is controlled by the physical processes of surface forcing, mixing and advection, DIC reflects both physical and biological processes because it is also impacted by photosynthesis, respiration, remineralization, and shell calcification. Budgets of DIC fluxes in the upper 20 m (Fig. 8) show that two major processes dominate, vertical circulation (light blue lines) and net biological processes (green lines). In the entire domain and all sub-regions, vertical circulation (advection and mixing) acts as a source of DIC, with the sum of all biological processes acting as a sink (n.b. the top 20 m does not constitute the entire euphotic zone, so respiration and remineralization at depth is not included). Maximum magnitudes of both vertical circulation and biological flux occur during the summer monsoon for all regions, except for the North AS where they occur during the winter monsoon bloom (Fig. 8c). Biological fluxes are nearly phase-matched with vertical circulation, though peaks in summer biological flux lag vertical circulation by a month (Fig. 8d,e,f). Comparing the two flux terms, after normalizing biological flux by vertical circulation flux, the relative strength of biological processes versus

https://doi.org/10.5194/bg-2021-22
Preprint. Discussion started: 17 February 2021

vertical sources of DIC becomes apparent. In the whole domain, biological flux ranges from -90% to -34.5% of vertical flux. As a result, biological fixation of carbon is generally weaker than physical vertical delivery of DIC.

Air-sea flux (red lines) is always negative due to the high pCO_2 values, peaking during the summer monsoon. DIC flux due to atmospheric escape is mostly smaller than biological flux, with the exception of spring when primary productivity is weak and pCO_2 values are high. Evaporation and precipitation (brown lines) results in higher DIC for most of the year (i.e. net evaporation) in the entire domain and upwelling regions, except India where it is negative (net precipitation). The oligotrophic region's evaporation and precipitation flux (Fig. 8d) oscillates from being either positive or negative four times during the year, with magnitudes rivaling air-sea flux at times. Horizontal advection (dark blue lines) is negative on average for the whole domain, denoting net export (Fig. 8a). The same pattern occurs for all sub-regions except India with net horizontal import of surface DIC (Fig. 8f). The Oman upwelling region and the oligotrophic region experience positive peaks of horizontal import during the summer monsoon, though for Somalia this period is the maximum DIC export. The overall, total flux of DIC experiences a summer positive peak during the summer monsoon, except for the North AS which has its positive peak in winter.

Overall, the near-surface AS DIC budget provides a picture where the physical delivery and biological drawdown of DIC, which are both larger in magnitude than the air-sea CO_2 flux, compete to produce the annual cycle of DIC fluctuations. For all regions except for the North AS (where similar processes occur during the winter monsoon), the largest physical vertical fluxes occur during the summer monsoon when wind forcing both upwells subsurface water and produces mixing to enhance DIC. The biological drawdown of DIC occurs concurrently or slightly lags the physical circulation since subsurface nutrient delivery must occur before stimulating phytoplankton growth. Importantly, the magnitude of biological DIC drawdown is less than the sourcing from vertical circulation, limiting the prospect of biological control of pCO_2 in the AS.

3.4 Air-sea CO_2 flux and drivers of seasonal variability

Modeled annual mean atmospheric flux of CO_2 (Fig. 9a) shows outgassing (positive, red) throughout the entire domain, producing an average annual CO_2 flux density rate of 1.9 $\mathrm{mol\ C\ m^{-2}yr^{-1}}$ and a total of 162.6$\mathrm{TgC\ yr^{-1}}$. Similar to pCO_2, several hotspots appear in the geographic distribution. Near the coast of Oman, the average flux density is 2.7, with 3.2 in Somalia and 2.4 along the coast of India $\mathrm{mol\ C\ m^{-2}yr^{-1}}$, producing a flux of 11.4, 32.9, and 4.9 $\mathrm{TgCyr^{-1}}$, respectively. The other regions, the North AS and oligotrophic central AS, have average densities of 2.0 and 1.5 $\mathrm{mol\ C\ m^{-2}yr^{-1}}$, with total fluxes of 10.5 and 28.6 $\mathrm{TgCyr^{-1}}$. The seasonal air-sea flux (Fig 9b-e) has minima during fall and winter, with an increase in spring and a strong maximum during summer monsoon. Oman and Somalia flux densities during summer monsoon are 5.8 and 5.9 $\mathrm{mol\ C\ m^{-2}yr^{-1}}$, respectively. The distribution of enhanced summer air-sea CO_2 flux coincides with the southwest monsoon winds, as well as the band of cooler temperatures impacting spatial pCO_2 anomalies in Fig. 7c. The entire domain fluxes 32.0, 26.6, 90.9, and 13.1 $\mathrm{TgCyr^{-1}}$ for the winter, spring, summer, and fall periods, respectively, each contributing 19.7, 16.3, 55.9, and 8.1% of the annual total.

The variability in air-sea CO_2 flux can be attributed to the contributions of winds, pCO_2, and interacting cross-terms, as described in Eqn. (8). The temporal anomalies for the summer monsoon, the period with strongest CO_2 flux signal, are presented

https://doi.org/10.5194/bg-2021-22
Preprint. Discussion started: 17 February 2021

in Fig. 10. Most of the domain has positive anomalies in air-sea flux (Fig. 10a). The wind contribution to flux variability, $\kappa\alpha$ (Fig. 10b), is also positive in most of the domain except the Gulf of Aden and the south-eastern corner of the domain, with its magnitude and distribution close to the total anomaly in Fig. 10a. The ΔpCO_2 contribution to seasonal flux anomaly (Fig. 10c) has a lower magnitude effect overall, with positive values north of 10^oN and slightly negative to the south. Maxima in these values occur near the upwelling centers of Oman, Somalia, and the Indian coast. Second-order cross-term values (Fig. 10d) are almost all positive, with maxima also occurring near upwelling centers similar to the ΔpCO_2 term but weaker in magnitude.

The seasonal flux anomalies for all regions throughout the year are displayed in Fig. 11. The summer monsoon flux is so strong that it makes the anomalies (purple bars) for all the other seasons in all regions negative, except for the spring in the North AS and central oligotrophic AS. During the winter months DJFM, both wind and pCO_2 terms produce negative flux anomalies, indicating the relative lack of winds and minimum pCO_2 values in the domain. In winter, while the negative wind term is universally strongest, within the upwelling regions the pCO_2 term is 58% of the wind term's magnitude, and 53% for the entire domain. The spring intermonsoon, where many regions such as Somalia and the central oligotrophic AS experience their pCO_2 maximum, shows a positive pCO_2 effect on flux anomaly that is as large as or larger than the negative wind effect. In the oligotrophic region, the second-order cross-term is small enough so that the net result is a positive anomaly, while in Somalia the near-balance between winds and pCO_2 make the cross-terms important in creating a negative anomaly. Summer monsoon winds represent the majority contribution to CO_2 flux variability, with a minimum 64.7% contribution relative to the total anomaly in India, a maximum of 112.8% in the oligotrophic AS, and 90.8% for the whole domain. By contrast, summer pCO_2 and cross-terms contribute 6.0 and 3.1% to the domain's anomaly, respectively. Fall inter-monsoon months resemble the winter monsoon, with negative wind anomalies contributing most with small or negative pCO_2 contributions. In most scenarios, pCO_2 contributes in the same direction as the winds or little at all, with the notable exceptions of Oman, oligotrophic AS, Somalia, and the domain during spring inter-monsoon.

In summary, the air-sea CO_2 flux is positive throughout the domain for the entire year, producing a total 162.6 TgCyr^{-1}, and is particularly elevated near the upwelling regions during the summer monsoon. Seasonal variability in flux is driven primarily by the strong onset of summer monsoon winds.

4 Discussion

4.1 Model pCO_2 vs. data

The pCO_2 output from the model has a positive bias with respect to the *in situ* data, as is clear from Fig. 3-5. The question becomes whether the model bias precludes its use in acquiring a reasonable air-sea CO_2 flux estimate. Regarding the direction of CO_2 flux (positive outgassing or negative uptake), the data in Fig. 2 are clear that, to the extent that *in situ* data exist and provide good coverage, ΔpCO_2 values are mostly positive (90%). Additionally, the bias is negative in the summer months, when the overall highest pCO_2 data values occur, and also when CO_2 flux peaks due to monsoon winds. Therefore, the positive bias in model pCO_2 should not significantly change the overall direction of flux, and the model results reaffirm the previous findings of Sarma et al. (1998) and subsequent work demonstrating that the AS is a source of CO_2 to the atmosphere.

https://doi.org/10.5194/bg-2021-22
Preprint. Discussion started: 17 February 2021

A positive bias in model pCO_2 has been noted in previous modeling studies. For instance, in the global data assimilation study of Valsala and Maksyutov (2010), they found an overall positive bias in the North Indian ocean, with a similar underestimate near the upwelling regions (summer negative bias in the model) of the AS and overestimate elsewhere (their Figures 3 and 4). In Sreeush et al. (2019a), ROMS resulted in systematic positive pCO_2 bias, whereas the offline Ocean Transport Tracer Model (OTTM) produced negative bias in pCO_2 in comparison to TK09. Anomalous patterns can be seen in OTTM, as well, with a maximum pCO_2 found near the equator as opposed to near the Oman coast (Valsala and Murtugudde, 2015).

The search for the model bias source is hindered by the lack of *in situ* data in the region. While the bias does not appear to be from T and S, but rather DIC and TA (Fig. S4), it is difficult to pinpoint which processes create these discrepancies since in the AS domain the GLODAP database has a total of 334 locations where both DIC and TA are sampled in the upper $50\mathrm{m}$ of the water column. The few available *in situ* data that *do* exist in the AS have a number of deficiencies for the purpose of validating model output. First, the data available are both old and concentrated around the years 1995 and 1997. While the JGOFS studies were quintessential in diagnosing the seasonal cycle of pCO_2, they preclude being able to decipher the secular trend in surface pCO_2 due to increasing atmospheric CO_2 concentrations. In our analysis, we estimated a $+2\mu\mathrm{atm\ yr}^{-1}$ trend, close to that of Tjiputra et al. (2014), though finding an inter-annual linear trend requires more data at regular intervals. Second, due to the nature of strong upwelling in the AS, previous cruise sampling also biases not only the summer months (≈70% of data), but also in the vicinity of the Oman coast (Fig. 3c). As a result, it is difficult to determine to what extent the data are representative of the entire AS. Consider that in the model, flux intensities are lower in the central, oligotrophic region (Fig. 10), but due to its surface area the total flux ($28.6\ \mathrm{TgCyr}^{-1}$) was close to that of Somalia ($32.9\ \mathrm{TgCyr}^{-1}$), an observation also made by Lendt et al. (2003). Determining to what extent the model over- or under-estimates CO_2 flux due to pCO_2 bias would require more *in situ* sampling, which would need to be designed around solving the problems of areal coverage (outside of Oman and upwelling zones) and temporal coverage (off-summer months and recurrent over multiple years).

Despite the model's limitations, its advantages are also clear. Beyond the obvious increase in spatio-temporal coverage, capturing the monsoon's strong seasonal dynamics helps the model where other approaches fall short. This is especially illustrated in Fig. 5. Since upwelling regions are limited in geographic extent near the coast, capturing their high pCO_2 values can be difficult for other approaches, such as TK09 with its coarse grid. Even the L15 product, with its finer grid, is unable to produce the higher pCO_2 values seen during the summer. Judging from these comparisons, the trade-off appears to be that the model currently may produce less accurate pCO_2 values outside of summer, but the explicit resolving of upwelling allows for enhanced pCO_2 values during the summer monsoon, the peak of CO_2 flux.

4.2 Surface distribution of pCO_2 and spatial, temporal anomalies

The distribution of model pCO_2 is both similar to and different from previous studies. Apart from the aforementioned bias leading to heightened absolute values (though Bates et al. (2006) has >400 $\mu\mathrm{atm}$ for large parts of the AS), the relatively enhanced pCO_2 values near Oman, along the west coast of India, and in the Gulf of Aden have already been observed (Sabine et al., 2000; Bates et al., 2006; Sarma et al., 2000). These same studies, however, note a minimum of pCO_2 outside of the summer monsoon near the south-west coast of India due to freshwater influx, which is not replicated well in the model.

https://doi.org/10.5194/bg-2021-22
Preprint. Discussion started: 17 February 2021


Biogeosciences Discussions Open Access EGU

Additionally, elevated pCO_2 near the equator is not observed (Sabine et al., 2000; Bates et al., 2006), although as already noted it can appear in other models (Valsala and Murtugudde, 2015). The model's seasonal pCO_2 minimum during the winter monsoon is also not reflective of results found elsewhere (Goyet et al. (1998a, b); Bates et al. (2006); though many studies highlight the North AS, where minimum model pCO_2 occurs during the spring). Instead, these papers state pCO_2 is minimal during the fall inter-monsoon. Likewise, the large-scale spring maximum of pCO_2 seen in the model is not found in these studies, except for in Louanchi et al. (1996), though this result is somewhat anomalous since that study showed a pCO_2 minimum during summer monsoon. Thus, while the model agrees with previous work insofar as the coastal regions impacted by upwelling show enhanced pCO_2, mismatches do appear in the seasonal timing of maxima and minima, especially within certain sub-regions.

The spatial decomposition of factors influencing pCO_2 (Fig. 6) highlights how geographically DIC can be the strongest factor, with temperature and TA taking secondary roles and freshwater being a weak contributor. Since DIC and TA can co-vary with salinity, when they are not normalized their distribution in the AS mirrors the north-south salinity gradient (see figures 2,3 in Bates et al. (2006)). Once corrected for salinity, it is clear that the upwelling region of Oman still has elevated DIC whereas the central, oligotrophic AS shows a DIC deficit. By contrast, the onshore-offshore gradient in TA is weaker. Differences between coastal and offshore normalized DIC and TA in the AS have been previously observed (Millero et al., 1998b; Lendt et al., 2003), but the stronger relative absence of DIC in the central AS and its role in determining pCO_2 has not been emphasized. A similar analysis in the California Current upwelling system (Turi et al., 2014) indicates near-compensation of DIC and temperature in opposing directions, nearly overlapping each other. In that scenario, DIC overpowers temperature at the coast, with TA and freshwater being secondary. For the AS, while the upwelling regions of Oman and Somalia show temperature and DIC working against each other, they are not as well compensated. Furthermore, the gradients of positive/negative pCO_2 contributions from temperature and DIC do not overlap, leading to the curious scenario where temperature and DIC both contribute positively to the pCO_2 anomaly along the Indian coast. The positioning of these gradients and the surprising negative influence of DIC away from upwelling regions perhaps underscores how the AS is rather unique, where strong seasonal upwelling winds mingle with strong tropical heating and the influence of outflows from marginal seas.

Decomposition of seasonal pCO_2 anomalies within regions portrays a slightly different picture where temperature is the dominant force, with DIC countervailing in the upwelling regions. Not only is this seasonal cycle more akin to that seen in the California Current (Turi et al., 2014), the dueling role of these two forces is also reflected in a similar analysis by Sreeush et al. (2019a) for pH instead of pCO_2 in the AS. Interestingly, in that study both ROMS and OTTM were compared side-by-side, and in OTTM, TA played a larger role than in ROMS. Similarly, in Valsala and Maksyutov (2013), TA played an important role in regulating inter-annual pCO_2 variability in the AS. These results using another model raise the possibility that TA's importance is under-estimated in the current study.

Zooming out from the upwelling regions and looking at the whole AS, the dominance of temperature is clear. This observation, temperature overriding DIC in the AS to determine temporal pCO_2 changes, can also be seen in the interannual variability analysis of Doney et al. (2009). In the domain average, temperature effects nearly overlap with the overall pCO_2 anomaly. This result brings back into focus the seasonal timing of pCO_2 minima/maxima in the model vis à vis previous work.

https://doi.org/10.5194/bg-2021-22
Preprint. Discussion started: 17 February 2021

In the earlier studies, which either use data directly or build statistical models from those data, there is no spring intermonsoon pCO_2 maximum driven by heating. Indeed, Sabine et al. (2000) noted that pCO_2 in the spring was much lower than would be expected given the SST, but attributed this to drawdown due to biological production. The model, however, indicates that this is precisely the season where biological production is at its lowest. The presence of these springtime maxima can be seen in other models, visible in the results of Valsala and Maksyutov (2010) and a synthesis by Sarma et al. (2013). Since the model indicates temperature is producing the maxima, it reduces the concern that erroneous DIC or TA values in the model are driving this signal. The model SST matches well with the *in situ* data (Fig. S4), and the forcing datasets for SST and heat flux correspond to data that predate or include the pCO_2 sampling period (i.e. before 2000), so a climate change bias is unlikely. What might be more likely, then, is a sampling bias towards summertime Oman, one of the few areas in the AS with a summertime instead of springtime pCO_2 max. Such a bias could possibly obscure what is happening in the rest of the AS. Regardless, the discrepancy between models and observations during the spring period can be added as yet another reason to conduct more *in situ* sampling to either confirm or disavow whether the model results are spurious.

4.3 DIC seasonal budget and driving mechanisms

The potential for biological control in setting pCO_2 has been found in Sri Lanka near the AS (Chakraborty et al., 2018). In this study, it was found that the source water in Sri Lanka was sufficiently low in DIC relative to inorganic nutrients that upwelling actually reduced surface pCO_2. In a similar vein, Takahashi et al. (2002) found, using a metric comparing temperature and "biological" effects (i.e. everything else), that the AS's pCO_2 is reduced more by biological production than temperature effects. Conducting this analysis on the model output (Fig. S5), it appears that "biological" control appears dominant over the upwelling areas (Oman coast, coast of Somalia, India) and near the equator east of 60^oE, but for the majority of the AS temperature dominates. This cursory analysis aside, as is evident in the results of Chakraborty et al. (2018), the more useful comparison is in determining whether biological production is sufficient to outweigh DIC enhancement from subsurface water.

In summary, the results in Fig. 8 indicate that for the entire AS, DIC enhancement by vertical circulation (both advection and mixing) brings more DIC into the near-surface than is removed by net biological processes, and so no biologically-induced decrease of pCO_2 occurs. The timing of biological drawdown, occurring at the same time or lagging vertical circulation, is consistent with the general phenology of blooms and similar to previous findings (Louanchi et al., 1996; Rixen et al., 2006; Sharada et al., 2008). The result that biological cycling of carbon is much larger than the air-sea flux of CO_2 also corroborates the results of Lendt et al. (2003), who found net community production to be $\approx$3.6 times larger than CO_2 emission. The relatively low impact of horizontal advection is an interesting detail to consider; in other upwelling systems, significant proportions of water and biological production are advected offshore (Nagai et al., 2015). Lendt et al. (2003) suggest upwelled nitrate is assimilated and does not arrive in the central AS, while Resplandy et al. (2011) show that a large fraction of total nutrients in the central AS come from the upwelling zones. Thus, although water may be advected offshore, the relevant timescale for DIC cycling processes (i.e. air-sea emission, biological uptake) may be short enough so that horizontal export of enhanced DIC (keep in mind the onshore-offshore normalized DIC gradient) from the upwelling regions does not significantly contribute to the central AS or other regions.

https://doi.org/10.5194/bg-2021-22
Preprint. Discussion started: 17 February 2021

4.4 Variability and mechanisms controlling air-sea CO_2 flux

4.4.1 Flux distribution, seasonality, and drivers

The model results both affirm the conclusions of previous studies in terms of CO_2 flux direction and seasonality, yet find difference in magnitudes. As previously stated, the AS is a atmospheric CO_2 source, with most flux occurring (56%) during the summer monsoon (Fig. 9). In our results, however, there is no region during any of the seasons where uptake of CO_2 takes place. While somewhat expected, this is still in disagreement with some of the other pCO_2 datasets previously considered, such as in Sarma (2003), where negative ΔpCO_2 values appear, such as during winter monsoon near the south coast of India. The model's positive pCO_2 bias may be to blame for this, making it so that no negative ΔpCO_2 appears. Despite the positive pCO_2 bias, a few other patterns are clear in comparison to other CO_2 flux estimates. Sabine et al. (2000) and Sarma (2003) both find the maximum flux occurring during the summer monsoon centered around the upwelling regions, which is also quite visible in the model results (Fig. 10d). However, Bates et al. (2006) found that a secondary maximum of flux occurs during the winter monsoon, though due to the color scale in their figure 6 it is difficult to ascertain much beyond CO_2 outgassing from the AS during all months of the year. Their secondary max in flux may be partly attributable to higher wintertime pCO_2, as well.

The fact that model CO_2 flux peaks in summer despite a wide-ranging spring peak in pCO_2 is the first sign that perhaps pCO_2 is not the primary driver in determining flux timing. The Reynolds decomposition of CO_2 flux terms (Fig. 10) clearly shows that a large proportion of the summer flux is due to the arrival of the strong SW summer monsoon winds. The positive contributions due to pCO_2 occur in the usual upwelling regions, though their contribution in magnitude is relatively muted, and negative in the southern portion of the AS. Cross-terms, while non-zero, are inconsequential in determining the overall anomaly in summer flux intensity, as has been seen elsewhere (Doney et al., 2009). Indeed, one of the largest cross-term contributions is in Oman during the summer (Fig. 11), but this clearly is not enough to sway the direction of the anomaly. The summer flux signal is so strong that in nearly all the regions outside of summer, the anomaly is negative (Fig. 11). Furthermore, the contribution of winds in particular is so strong, it is the largest factor all year except for the spring intermonsoon, where peak pCO_2 is important relative to the effects of wind (or lack thereof) in the central oligotrophic AS, Somalia, and the averaged domain. This would suggest that, on first order, winds are the most important factor in determining the seasonal air-sea flux cycle in the AS, to the point that wind contribution to the domain's summer anomaly was 90.8% in magnitude relative to the total. Therefore, when considering the inconsistencies of models in estimating air-sea CO_2 flux (Sarma et al., 2013), the possibility that incomplete representation of winds and the various parameterizations of piston velocity must be considered in addition to pCO_2.

4.4.2 Influence of variable pCO_2 in flux magnitude

While strong monsoon winds dominate the timing of air-sea CO_2 flux, and the AS is always a source of CO_2 due to mostly positive ΔpCO_2, the variability in pCO_2 between independent sources can still result in a wide range of overall magnitudes. In the AS, CO_2 outgassing estimates vary from 7 TgCyr^{-1} (Goyet et al., 1998b) to >90 TgCyr^{-1} (Sarma, 2003), with each study using their own pCO_2 data and wind parameterizations. Considering the important role of winds, the best way to investigate the

https://doi.org/10.5194/bg-2021-22
Preprint. Discussion started: 17 February 2021

role of pCO_2 variability is to keep winds (and their flux parameterization) constant. Towards this end, we use multiple pCO_2 products to calculate CO_2 flux with the same winds and parameterization as the model (Fig. 12). As summarized in Table 1, pCO_2 from TK09, L15, GLODAP data and Sarma (2003), interpolated to the WOA 1^ox1^o grid, were used in these calculations (except for TK09 where the coarse resolution reduced coverage). The original applicability of the Sarma (2003) model is north of 10^oN, and so flux was calculated for this region, as well.

Despite differing pCO_2 seasonality (Fig. 5), all calculations have their peak CO_2 flux sometime in the summer, confirming the role of winds in CO_2 flux timing. After calculating total flux for both the entire AS and the Sarma (2003) reduced domain, this study's model consistently produced one of the higher estimates (except for GLODAP in the reduced domain; Fig. 12b). This is perhaps unsurprising, considering the pCO_2 bias. The ratio between the largest and smallest estimates of total CO_2 flux is 2.1 (57-120 TgCyr^{-1}) for the whole domain, and 5.3 (12.3 and 65.6 TgCyr^{-1}) for the reduced domain. It should be noted that application of the Sarma (2003) model resulted in negative ΔpCO_2 values. While some negative values were reported in the original publication, the total fluxes (12.3 or 17.6 TgCyr^{-1}) were quite smaller than the 70 TgCyr^{-1} reported using the same parameterization from Wanninkhof (1992). Removing the two Sarma models from the reduced domain analysis produces a ratio of 1.6 between the largest and smallest flux values, more in line with the whole domain's variability. Additionally, the GLODAP data, with no temporal variability in pCO_2, probably over-estimate pCO_2 and hence flux due to sampling bias near Oman during the summer monsoon, and so the ratio between flux estimates may indeed be smaller. As a final note, another interesting detail concerns how the original estimate of Sarma (2003) at 70 TgCyr^{-1} is larger than both the model, which had 57.1 TgCyr^{-1}, and GLODAP data. Thus, while the model pCO_2 bias makes us think the model over-estimates flux, it is still within the range of previous studies in the AS.

Ultimately, once winds are controlled, it appears that on balance: 1) gridded data-based pCO_2 products will under-estimate the upwelling zone maxima of pCO_2 and CO_2 flux during the summer, 2) the model over-estimates pCO_2 the rest of the year, eventually contributing to a possible over-estimate of CO_2 flux, and 3) this leaves reality somewhere in between. The only way to rectify these differences and arrive at a more accurate estimate will be to conduct sufficient *in situ* sampling of DIC, TA, and pCO_2 in more regions than the upwelling zones, and preferably outside of the summer and over the course of multiple years. With the advent of ARGO floats with pH sensors, and the advancement of technology for other variables such as TA, the possibility emerges of using autonomous sampling platforms to expand beyond the limitations of ship-board measurements to fill the data gap in the AS carbon system.

5 Conclusions

In this study, we used a regional circulation model coupled with a biogeochemical model to investigate the annual magnitude, seasonal cycle, and drivers of air-sea CO_2 flux in the AS, primarily winds and pCO_2. This effort was made to complement previous flux estimates, where limited data or insufficient model resolution have produced contrasting results. Consistent with previous work, we find that the AS is a source of CO_2 to the atmosphere for the entire year, with the bulk occurring during the summer monsoon. Our estimate of flux, $\approx$160 TgCyr^{-1}, with concentrated flux densities up to 6 $\mathrm{molCm}^{-2}\mathrm{yr}^{-1}$ in the

https://doi.org/10.5194/bg-2021-22
Preprint. Discussion started: 17 February 2021

upwelling regions, is larger than most previous reports but not inconsistent with the range of other findings. Since the AS lacks carbon data, here we subjected the model to validation with raw data instead of smoothed climatologies. The model is shown to have a positive bias in pCO_2, attributed to TA and DIC, with TA bias being stronger. Despite this, pCO_2 variability compares favorably to alternative products in the region. The bias results in strongly positive ΔpCO_2 throughout the domain year-round. While positive ΔpCO_2 values have been observed before in the AS, we likely over-estimate CO_2 flux outside of the summer monsoon.

The majority of flux occurs during the summer as opposed to a modeled spring pCO_2 maximum due to the influence of winds. A Reynolds decomposition of both pCO_2 and wind variability shows that the intense winds of the summer monsoon contribute 90% of that season's flux anomaly. In fact, winds play a more important role than the increase of pCO_2 in the upwelling regions. Even though winds represent such a major variable in determining AS CO_2 flux *timing*, the variability in *total* flux due to different pCO_2 products leads to a 2x range in magnitude. These results suggest that in addition to the expected increase of surface ocean pCO_2 due to anthropogenic climate change, possible changes in the timing, location, and magnitude of monsoon winds (Lachkar et al., 2018; Praveen et al., 01 Apr. 2020) will have downstream impacts on seasonal air-sea flux.

An important result of this modeling study is that temperature drives a springtime maximum of pCO_2 in the AS. This maximum has been observed in lower-resolution models, but is not found in the *in situ* data. Due to the fact that temperature is not sensitive to biological processes like DIC and TA, this discrepancy suggests that more sampling is necessary to determine whether it is an artifact of spotty sampling or an inherent problem in models unrelated to resolving coastal upwelling. Additionally, we find that spatial gradients of DIC and temperature do not overlap as they do elsewhere in the ocean. Instead, temperature follows a southwest-northeast monsoon wind pattern, whereas DIC is enhanced nearest to the coasts. The resulting apparent deficit of normalized DIC in the central, oligotrophic AS has not been emphasized previously. Finally, we find that despite the intense biological activity in the AS, primary production by phytoplankton is insufficient to counter the increased carbon supply provided by vertical circulation during bloom periods.

Models can be used to expand spatiotemporal coverage when data is scarce. However, models' limitations often manifest when there is no new data to test their fidelity. Limitations in the spatiotemporal coverage of existing datasets stem from biases in sampling during summer monsoon, sampling close to the Oman upwelling region, and limited in scope to the years of JGOFS expeditions of the 1990s. In order to fully characterize the pCO_2 cycle outside of summer in the rest of the AS, as well as to determine the secular trend of surface pCO_2 due to anthropogenic carbon additions to the atmosphere, more *in situ* data of the carbon system (e.g. DIC, TA, pCO_2), from shipboard measurements or autonomous sampling platforms, are sorely needed. Furthermore, since ΔpCO_2 is generally positive in the AS, the direction of air-sea CO_2 exchange examined here is robust to model error, whereas other important indicators such as pH and its relevant biological thresholds will be less so. These data are thus critical for resolving the possible responses of the carbon system in the AS to ongoing climate change, whether from changes in timing or magnitude of monsoon wind forcing, the impact of increased surface heating on stratification and vertical circulation, or changing levels of primary and fisheries productivity with altered carbonate solubility. Without this baseline information, it will be difficult to predict what the future has in store for the AS carbon system.

https://doi.org/10.5194/bg-2021-22
Preprint. Discussion started: 17 February 2021


Biogeosciences Discussions Open Access EGU

Competing interests. The authors declare that they have no competing financial interests.

Acknowledgements. Support for this research comes from the Center for Prototype Climate Modeling (CPCM), the New York University Abu Dhabi (NYUAD) Research Institute. Computations were conducted at the High Performance cluster (HPC) at NYUAD, Dalma. We deeply thank both B. Marchand and M. Barwani for their technical support.

https://doi.org/10.5194/bg-2021-22
Preprint. Discussion started: 17 February 2021

References

Bakker, D. C., Pfeil, B., Landa, C. S., Metzl, N., O'brien, K. M., Olsen, A., Smith, K., Cosca, C., Harasawa, S., Jones, S. D., et al.: A multi-decade record of high-quality fCO (2) data in version 3 of the Surface Ocean CO2 Atlas (SOCAT), Earth System Science Data, 8, 383–413, 2016.

Bates, N. R., Pequignet, A. C., and Sabine, C. L.: Ocean carbon cycling in the Indian Ocean: 1. Spatiotemporal variability of inorganic carbon and air-sea CO2 gas exchange, Global Biogeochemical Cycles, 20, https://doi.org/10.1029/2005GB002491, https://agupubs.onlinelibrary.wiley.com/doi/abs/10.1029/2005GB002491, 2006.

Carton, J. A. and Giese, B. S.: A reanalysis of ocean climate using Simple Ocean Data Assimilation (SODA), Monthly weather review, 136, 2999–3017, 2008.

Casey, K. S. and Cornillon, P.: A comparison of satellite and in situ–based sea surface temperature climatologies, Journal of Climate, 12, 1848–1863, 1999.

Chakraborty, K., Valsala, V., Gupta, G., and Sarma, V.: Dominant biological control over upwelling on pCO2 in sea east of Sri Lanka, Journal of Geophysical Research: Biogeosciences, 123, 3250–3261, 2018.

Ciais, P., Sabine, C., Bala, G., Bopp, L., Brovkin, V., Canadell, J., Chhabra, A., DeFries, R., Galloway, J., Heimann, M., et al.: Climate change 2013: the physical science basis. Contribution of Working Group I to the Fifth Assessment Report of the Intergovernmental Panel on Climate Change, K., Tignor, M., Allen, SK, Boschung, J., Nauels, A., Xia, Y., Bex, V., Midgley, PM, Eds, 2013.

da Silva, A. M., Young, C. C., and Levitus, S.: Atlas of surface marine data 1994, Vol. 4: Anomalies of fresh water fluxes, NOAA Atlas, NESDIS, 9, 1994.

Dickson, A. and Millero, F. J.: A comparison of the equilibrium constants for the dissociation of carbonic acid in seawater media, Deep Sea Research Part A. Oceanographic Research Papers, 34, 1733–1743, 1987.

Doney, S. C., Lima, I., Feely, R. A., Glover, D. M., Lindsay, K., Mahowald, N., Moore, J. K., and Wanninkhof, R.: Mechanisms governing interannual variability in upper-ocean inorganic carbon system and air–sea CO2 fluxes: Physical climate and atmospheric dust, Deep Sea Research Part II: Topical Studies in Oceanography, 56, 640–655, 2009.

Goyet, C., Metzl, N., Millero, F., Eischeid, G., O'sullivan, D., and Poisson, A.: Temporal variation of the sea surface CO2/carbonate properties in the Arabian Sea, Marine Chemistry, 63, 69–79, 1998a.

Goyet, C., Millero, F. J., O'Sullivan, D., Eischeid, G., McCue, S., and Bellerby, R.: Temporal variations of pCO2 in surface seawater of the Arabian Sea in 1995, Deep Sea Research Part I: Oceanographic Research Papers, 45, 609–623, 1998b.

Gruber, N., Frenzel, H., Doney, S. C., Marchesiello, P., McWilliams, J. C., Moisan, J. R., Oram, J. J., Plattner, G.-K., and Stolzenbach, K. D.: Eddy-resolving simulation of plankton ecosystem dynamics in the California Current System, Deep Sea Research Part I: Oceanographic Research Papers, 53, 1483–1516, 2006.

Gruber, N., Lachkar, Z., Frenzel, H., Marchesiello, P., Münnich, M., McWilliams, J. C., Nagai, T., and Plattner, G.-K.: Eddy-induced reduction of biological production in eastern boundary upwelling systems, Nature geoscience, 4, 787–792, 2011.

Gruber, N., Hauri, C., Lachkar, Z., Loher, D., Frölicher, T. L., and Plattner, G.-K.: Rapid progression of ocean acidification in the California Current System, science, 337, 220–223, 2012.

Hauri, C., Gruber, N., Vogt, M., Doney, S. C., Feely, R. A., Lachkar, Z., Leinweber, A., McDonnell, A. M., Münnich, M., and Plattner, G.-K.: Spatiotemporal variability and long-term trends of ocean acidification in the California Current System, Biogeosciences, 10, 193–216, 2013.

https://doi.org/10.5194/bg-2021-22
Preprint. Discussion started: 17 February 2021

Hood, R. R., Urban, E. R., McPhaden, M. J., Su, D., and Raes, E.: The 2nd International Indian Ocean Expedition (IIOE-2): Motivating New Exploration in a Poorly Understood Basin., Limnology and Oceanography Bulletin, 25, 117–124, 2016.

Keeling, C. D.: Carbon dioxide in surface ocean waters: 4. Global distribution, Journal of Geophysical Research (1896-1977), 73, 4543–4553, https://doi.org/10.1029/JB073i014p04543, https://agupubs.onlinelibrary.wiley.com/doi/abs/10.1029/JB073i014p04543, 1968.

Keeling, C. D., Brix, H., and Gruber, N.: Seasonal and long-term dynamics of the upper ocean carbon cycle at Station ALOHA near Hawaii, Global Biogeochemical Cycles, 18, 2004.

Khatiwala, S., Primeau, F., and Hall, T.: Reconstruction of the history of anthropogenic CO 2 concentrations in the ocean, Nature, 462, 346–349, 2009.

Kumar, S. P., Ramaiah, N., Gauns, M., Sarma, V., Muraleedharan, P., Raghukumar, S., Kumar, M. D., and Madhupratap, M.: Physical forcing of biological productivity in the Northern Arabian Sea during the Northeast Monsoon, Deep Sea Research Part II: Topical Studies in Oceanography, 48, 1115–1126, 2001.

Lachkar, Z. and Gruber, N.: Response of biological production and air–sea CO2 fluxes to upwelling intensification in the California and Canary Current Systems, Journal of Marine Systems, 109, 149–160, 2013.

Lachkar, Z., Smith, S., Lévy, M., and Pauluis, O.: Eddies reduce denitrification and compress habitats in the Arabian Sea, Geophysical Research Letters, 43, 9148–9156, 2016.

Lachkar, Z., Lévy, M., and Smith, S.: Intensification and deepening of the Arabian Sea oxygen minimum zone in response to increase in Indian monsoon wind intensity., Biogeosciences, 15, 2018.

Landschützer, P., Gruber, N., Haumann, F. A., Rödenbeck, C., Bakker, D. C., Van Heuven, S., Hoppema, M., Metzl, N., Sweeney, C., Takahashi, T., et al.: The reinvigoration of the Southern Ocean carbon sink, Science, 349, 1221–1224, 2015.

Large, W. G., McWilliams, J. C., and Doney, S. C.: Oceanic vertical mixing: A review and a model with a nonlocal boundary layer parameterization, Reviews of Geophysics, 32, 363–403, 1994.

Lee, K., Tong, L. T., Millero, F. J., Sabine, C. L., Dickson, A. G., Goyet, C., Park, G.-H., Wanninkhof, R., Feely, R. A., and Key, R. M.: Global relationships of total alkalinity with salinity and temperature in surface waters of the world's oceans, Geophysical Research Letters, 33, https://doi.org/10.1029/2006GL027207, https://agupubs.onlinelibrary.wiley.com/doi/abs/10.1029/2006GL027207, 2006.

Lendt, R., Thomas, H., Hupe, A., and Ittekkot, V.: Response of the near-surface carbonate system of the northwestern Arabian Sea to the southwest monsoon and related biological forcing, Journal of Geophysical Research: Oceans, 108, 2003.

Lévy, M., Shankar, D., André, J.-M., Shenoi, S., Durand, F., and de Boyer Montégut, C.: Basin-wide seasonal evolution of the Indian Ocean's phytoplankton blooms, Journal of Geophysical Research: Oceans, 112, 2007.

Louanchi, F., Metzl, N., and Poisson, A.: Modelling the monthly sea surface fCO2 fields in the Indian Ocean, Marine Chemistry, 55, 265–279, 1996.

Lovenduski, N. S., Gruber, N., Doney, S. C., and Lima, I. D.: Enhanced CO2 outgassing in the Southern Ocean from a positive phase of the Southern Annular Mode, Global Biogeochemical Cycles, 21, 2007.

Mahadevan, A., Lévy, M., and Mémery, L.: Mesoscale variability of sea surface pCO2: What does it respond to?, Global Biogeochemical Cycles, 18, https://doi.org/10.1029/2003GB002102, https://agupubs.onlinelibrary.wiley.com/doi/abs/10.1029/2003GB002102, 2004.

Mahadevan, A., Tagliabue, A., Bopp, L., Lenton, A., Mémery, L., and Lévy, M.: Impact of episodic vertical fluxes on sea surface pCO₂, Philosophical Transactions of the Royal Society A: Mathematical, Physical and Engineering Sciences, 369, 2009–2025, https://doi.org/10.1098/rsta.2010.0340, https://royalsocietypublishing.org/doi/abs/10.1098/rsta.2010.0340, 2011.

https://doi.org/10.5194/bg-2021-22
Preprint. Discussion started: 17 February 2021

Marchesiello, P., Debreu, L., and Couvelard, X.: Spurious diapycnal mixing in terrain-following coordinate models: The problem and a solution, Ocean Modelling, 26, 156–169, 2009.

Mehrbach, C., Culberson, C., Hawley, J., and Pytkowicx, R.: Measurement of the apparent dissociation constants of carbonic acid in seawater at atmospheric pressure 1, Limnology and oceanography, 18, 897–907, 1973.

Millero, F. J.: Thermodynamics of the carbon dioxide system in the oceans, Geochimica et Cosmochimica Acta, 59, 661–677, 1995.

Millero, F. J., Degler, E. A., O'Sullivan, D. W., Goyet, C., and Eischeid, G.: The carbon dioxide system in the Arabian Sea, Deep Sea Research Part II: Topical Studies in Oceanography, 45, 2225–2252, 1998a.

Millero, F. J., Lee, K., and Roche, M.: Distribution of alkalinity in the surface waters of the major oceans, Marine Chemistry, 60, 111 – 130, https://doi.org/https://doi.org/10.1016/S0304-4203(97)00084-4, http://www.sciencedirect.com/science/article/pii/S0304420397000844, 1998b.

Nagai, T., Gruber, N., Frenzel, H., Lachkar, Z., McWilliams, J. C., and Plattner, G.-K.: Dominant role of eddies and filaments in the offshore transport of carbon and nutrients in the C alifornia C urrent S ystem, Journal of Geophysical Research: Oceans, 120, 5318–5341, 2015.

Naqvi, S. W. A., Gupta, R. S., and Kumar, M. D.: Carbon dioxide and nitrous oxide in the Arabian Sea, Washington DC American Geophysical Union Geophysical Monograph Series, 75, 85–92, https://doi.org/10.1029/GM075p0085, 1993.

Naqvi, S. W. A., Bange, H. W., Gibb, S. W., Goyet, C., Hatton, A. D., and Upstill-Goddard, R. C.: Biogeochemical ocean-atmosphere transfers in the Arabian Sea, Progress in Oceanography, 65, 116–144, 2005.

Olsen, A., Lange, N., Key, R. M., Tanhua, T., Álvarez, M., Becker, S., Bittig, H. C., Carter, B. R., Cotrim da Cunha, L., Feely, R. A., van Heuven, S., Hoppema, M., Ishii, M., Jeansson, E., Jones, S. D., Jutterström, S., Karlsen, M. K., Kozyr, A., Lauvset, S. K., Lo Monaco, C., Murata, A., Pérez, F. F., Pfeil, B., Schirnick, C., Steinfeldt, R., Suzuki, T., Telszewski, M., Tilbrook, B., Velo, A., and Wanninkhof, R.: GLODAPv2.2019 – an update of GLODAPv2, Earth System Science Data, 11, 1437–1461, https://doi.org/10.5194/essd-11-1437-2019, https://essd.copernicus.org/articles/11/1437/2019/, 2019.

Orr, J. and Epitalon, J.-M.: Improved routines to model the ocean carbonate system: mocsy 2.0., Geoscientific Model Development, 8, 2015.

Orr, J. C., Epitalon, J.-M., Dickson, A. G., and Gattuso, J.-P.: Routine uncertainty propagation for the marine carbon dioxide system, Marine Chemistry, 207, 84–107, 2018.

Paulmier, A., Ruiz-Pino, D., and Garçon, V.: CO_2 maximum in the oxygen minimum zone (OMZ), Biogeosciences, 8, 239–252, https://doi.org/10.5194/bg-8-239-2011, https://bg.copernicus.org/articles/8/239/2011/, 2011.

Pfeil, B., Olsen, A., Bakker, D. C., Hankin, S., Koyuk, H., Kozyr, A., Malczyk, J., Manke, A., Metzl, N., Sabine, C. L., et al.: A uniform, quality controlled Surface Ocean CO 2 Atlas (SOCAT), Earth System Science Data, 5, 125–143, 2013.

Praveen, V., Valsala, V., Ajayamohan, R. S., and Balasubramanian, S.: Oceanic Mixing over the Northern Arabian Sea in a Warming Scenario: Tug of War between Wind and Buoyancy Forces, Journal of Physical Oceanography, 50, 945 – 964, https://doi.org/10.1175/JPO-D-19-0173.1, https://journals.ametsoc.org/view/journals/phoc/50/4/jpo-d-19-0173.1.xml, 01 Apr. 2020.

Resplandy, L., Lévy, M., Madec, G., Pous, S., Aumont, O., and Kumar, D.: Contribution of mesoscale processes to nutrient budgets in the Arabian Sea, Journal of Geophysical Research: Oceans, 116, 2011.

Resplandy, L., Lévy, M., and McGillicuddy Jr., D. J.: Effects of Eddy-Driven Subduction on Ocean Biological Carbon Pump, Global Biogeochemical Cycles, 33, 1071–1084, https://doi.org/10.1029/2018GB006125, https://agupubs.onlinelibrary.wiley.com/doi/abs/10.1029/2018GB006125, 2019.

Risien, C. M. and Chelton, D. B.: A global climatology of surface wind and wind stress fields from eight years of QuikSCAT scatterometer data, Journal of Physical Oceanography, 38, 2379–2413, 2008.

https://doi.org/10.5194/bg-2021-22
Preprint. Discussion started: 17 February 2021

Rixen, T., Goyet, C., and Ittekkot, V.: Diatoms and their influence on the biologically mediated uptake of atmospheric CO 2 in the Arabian Sea upwelling system, Biogeosciences, 3, 1–13, 2006.

Sabine, C., Wanninkhof, R., Key, R., Goyet, C., and Millero, F. J.: Seasonal CO2 fluxes in the tropical and subtropical Indian Ocean, Marine Chemistry, 72, 33–53, 2000.

Sarma, V.: Monthly variability in surface pCO2 and net air-sea CO2 flux in the Arabian Sea, Journal of Geophysical Research: Oceans, 108, 2003.

Sarma, V., Kumar, M. D., and George, M.: The central and eastern Arabian Sea as a perennial source of atmospheric carbon dioxide, Tellus B: Chemical and Physical Meteorology, 50, 179–184, 1998.

Sarma, V., Swathi, P., Kumar, M. D., Prasannakumar, S., Bhattathiri, P., Madhupratap, M., Ramaswamy, V., Sarin, M., Gauns, M., Ramaiah, N., et al.: Carbon budget in the eastern and central Arabian Sea: An Indian JGOFS synthesis, Global Biogeochemical Cycles, 17, 2003.

Sarma, V. V., S, S., Kumar, M. D., Gauns, M., and Madhupratap, M.: Seasonal controls on surface pCO 2 in the central and eastern Arabian Sea, Academy Proceedings in Earth and Planetary Sciences, 109, 471–479, http://proxy.library.nyu.edu/login?url=https://www.proquest.com/docview/214115753?accountid=12768, copyright - Indian Academy of Sciences 2000; Last updated - 2010-08-11; SubjectsTermNotLitGenreText - Arabian Sea, 2000.

Sarma, V. V. S. S., Lenton, A., Law, R. M., Metzl, N., Patra, P. K., Doney, S., Lima, I. D., Dlugokencky, E., Ramonet, M., and Valsala, V.: Sea–air CO_2 fluxes in the Indian Ocean between 1990 and 2009, Biogeosciences, 10, 7035–7052, https://doi.org/10.5194/bg-10-7035-2013, https://bg.copernicus.org/articles/10/7035/2013/, 2013.

Schott, F. A. and McCreary Jr, J. P.: The monsoon circulation of the Indian Ocean, Progress in Oceanography, 51, 1–123, 2001.

Sharada, M., Swathi, P., Yajnik, K., and Devasena, C. K.: Role of biology in the air-sea carbon flux in the Bay of Bengal and Arabian Sea, Journal of earth system science, 117, 429–447, 2008.

Shchepetkin, A. F. and McWilliams, J. C.: The regional oceanic modeling system (ROMS): a split-explicit, free-surface, topography-following-coordinate oceanic model, Ocean modelling, 9, 347–404, 2005.

Smith, S. L.: The Arabian Sea of the 1990s: New biogeochemical understanding, Progress in Oceanography, 2, 113–115, 2005.

Sreeush, M. G., Rajendran, S., Valsala, V., Pentakota, S., Prasad, K., and Murtugudde, R.: Variability, trend and controlling factors of Ocean acidification over Western Arabian Sea upwelling region, Marine Chemistry, 209, 14–24, 2019a.

Sreeush, M. G., Valsala, V., Santanu, H., Pentakota, S., Prasad, K., Naidu, C., and Murtugudde, R.: Biological production in the Indian Ocean upwelling zones-Part 2: Data based estimates of variable compensation depth for ocean carbon models via cyclo-stationary Bayesian Inversion., Deep Sea Research Part II: Topical Studies in Oceanography, p. 104619, 2019b.

Takahashi, T., Sutherland, S. C., Sweeney, C., Poisson, A., Metzl, N., Tilbrook, B., Bates, N., Wanninkhof, R., Feely, R. A., Sabine, C., et al.: Global sea–air CO2 flux based on climatological surface ocean pCO2, and seasonal biological and temperature effects, Deep Sea Research Part II: Topical Studies in Oceanography, 49, 1601–1622, 2002.

Takahashi, T., Sutherland, S. C., Wanninkhof, R., Sweeney, C., Feely, R. A., Chipman, D. W., Hales, B., Friederich, G., Chavez, F., Sabine, C., et al.: Climatological mean and decadal change in surface ocean pCO2, and net sea–air CO2 flux over the global oceans, Deep Sea Research Part II: Topical Studies in Oceanography, 56, 554–577, 2009.

Takahashi, T., Sutherland, S. C., and Kozyr, A.: Global Ocean Surface Water Partial Pressure of CO2 Database: Measurements Performed During 1957-2018 (LDEO Database Version 2018) (NCEI Accession 0160492)., https://doi.org/10.3334/cdiac/otg.ndp088(v2015), 2019.

Taylor, K. E.: Summarizing multiple aspects of model performance in a single diagram, Journal of Geophysical Research: Atmospheres, 106, 7183–7192, 2001.

https://doi.org/10.5194/bg-2021-22
Preprint. Discussion started: 17 February 2021

Tjiputra, J. F., Olsen, A., Bopp, L., Lenton, A., Pfeil, B., Roy, T., Segschneider, J., Totterdell, I., and Heinze, C.: Long-term surface pCO2 trends from observations and models, Tellus B: Chemical and Physical Meteorology, 66, 23 083, 2014.

Turi, G., Lachkar, Z., and Gruber, N.: Spatiotemporal variability and drivers of pCO2 and air–sea CO2 fluxes in the California Current System: an eddy-resolving modeling study, Biogeosciences, 11, 671–690, 2014.

Valsala, V. and Maksyutov, S.: Simulation and assimilation of global ocean pCO2 and air–sea CO2 fluxes using ship observations of surface ocean pCO2 in a simplified biogeochemical offline model, Tellus B: Chemical and Physical Meteorology, 62, 821–840, 2010.

Valsala, V. and Maksyutov, S.: Interannual variability of the air–sea CO 2 flux in the north Indian Ocean, Ocean Dynamics, 63, 165–178, 2013.

Valsala, V. and Murtugudde, R.: Mesoscale and intraseasonal air–sea CO2 exchanges in the western Arabian Sea during boreal summer, Deep Sea Research Part I: Oceanographic Research Papers, 103, 101–113, 2015.

Valsala, V., Sreeush, M. G., and Chakraborty, K.: The IOD Impacts on the Indian Ocean Carbon Cycle, Journal of Geophysical Research: Oceans, 125, e2020JC016 485, https://doi.org/https://doi.org/10.1029/2020JC016485, https://agupubs.onlinelibrary.wiley.com/doi/abs/10.1029/2020JC016485, e2020JC016485 2020JC016485, 2020.

Van Heuven, S., Pierrot, D., Rae, J., Lewis, E., and Wallace, D.: MATLAB program developed for CO2 system calculations, ORNL/CDIAC-105b. Carbon Dioxide Information Analysis Center, Oak Ridge National Laboratory, US Department of Energy, Oak Ridge, Tennessee, 530, 2011.

Vic, C., Roullet, G., Carton, X., and Capet, X.: Mesoscale dynamics in the Arabian Sea and a focus on the Great Whirl life cycle: A numerical investigation using ROMS, Journal of Geophysical Research: Oceans, 119, 6422–6443, https://doi.org/10.1002/2014JC009857, https://agupubs.onlinelibrary.wiley.com/doi/abs/10.1002/2014JC009857, 2014.

Wanninkhof, R.: Relationship between wind speed and gas exchange over the ocean, Journal of Geophysical Research: Oceans, 97, 7373–7382, 1992.

Weiss, R.: Carbon dioxide in water and seawater: the solubility of a non-ideal gas, Marine chemistry, 2, 203–215, 1974.

Wolf-Gladrow, D. A., Zeebe, R. E., Klaas, C., Körtzinger, A., and Dickson, A. G.: Total alkalinity: The explicit conservative expression and its application to biogeochemical processes, Marine Chemistry, 106, 287–300, 2007.

https://doi.org/10.5194/bg-2021-22
Preprint. Discussion started: 17 February 2021

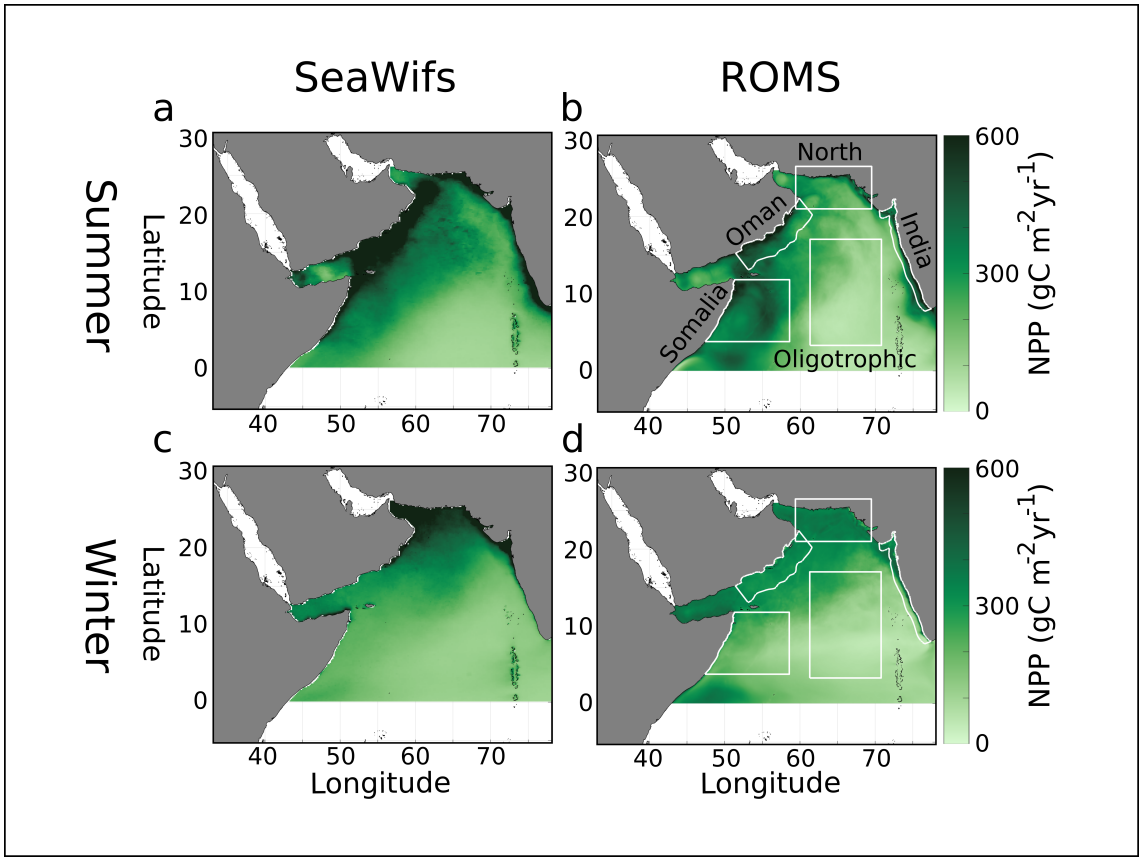

Figure 1. Vertically integrated net primary production in the Arabian Sea $\mathrm{gCm^{-2}yr^{-1}}$ from the VGPM algorithm (Behrenfeld and Falkowski, 1997) for SeaWifs (a,c) and model output (b,d) for the summer (JJAS, a-b) and winter (DJFM,c-d) monsoon. White boxes in (b,d) denote regions of analysis in the paper.

https://doi.org/10.5194/bg-2021-22
Preprint. Discussion started: 17 February 2021

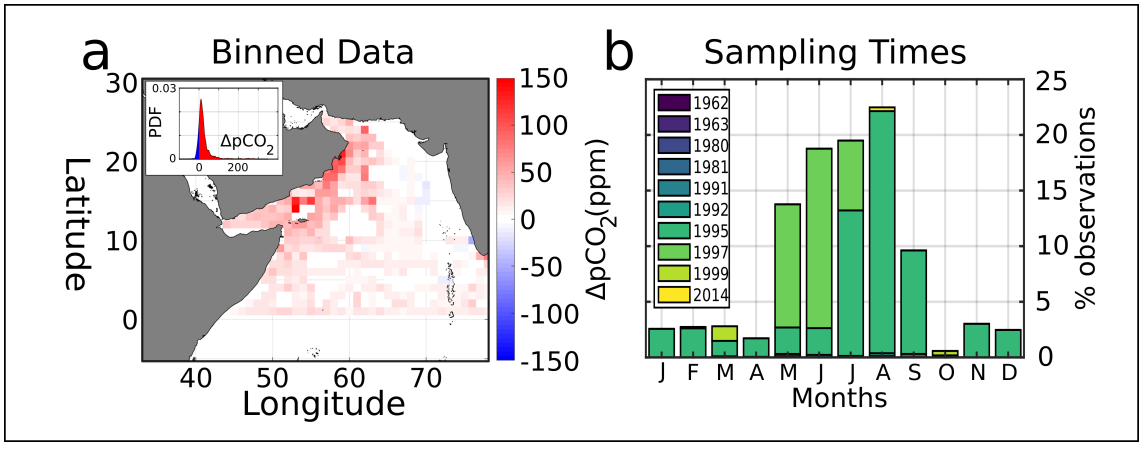

Figure 2. (a) Average surface *in situ* ΔpCO_2 (ppm), with probability density function (PDF) of all ΔpCO_2 values inset. ΔpCO_2 data are calculated in comparison to Keeling atmospheric pCO_2, then binned into a 1^ox1^o grid. (b) Monthly distribution of *in situ* data sampling times, color-coded by sampling year.

https://doi.org/10.5194/bg-2021-22
Preprint. Discussion started: 17 February 2021

Biogeosciences
Discussions
Open Access
EGU

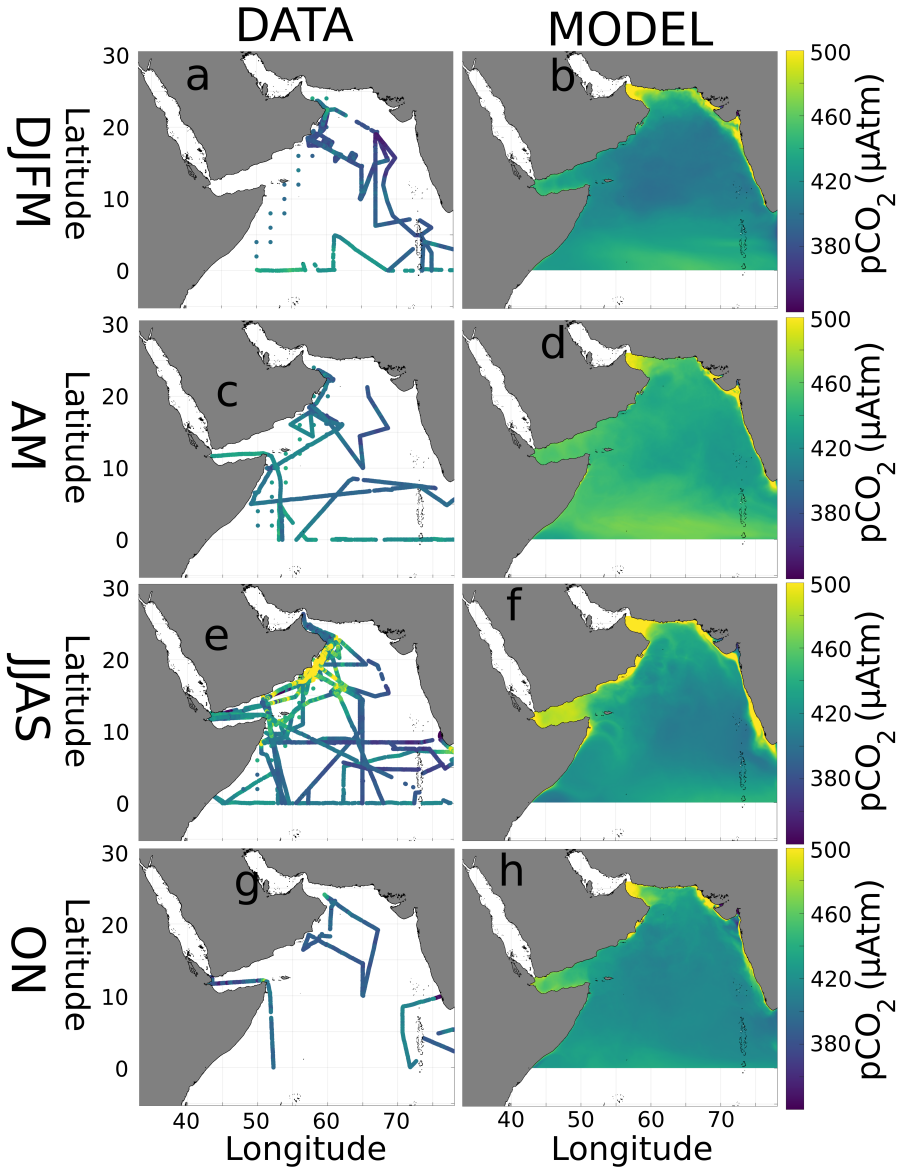

Figure 3. Seasonal surface pCO_2 (μatm) from data (a-d) and the model (e-h), representing winter monsoon DJFM (a,e), spring intermonsoon AM (b,f), summer monsoon JJAS (c,g), and fall intermonsoon ON (d,h).

https://doi.org/10.5194/bg-2021-22
Preprint. Discussion started: 17 February 2021

Biogeosciences
Discussions
Open Access
EGU

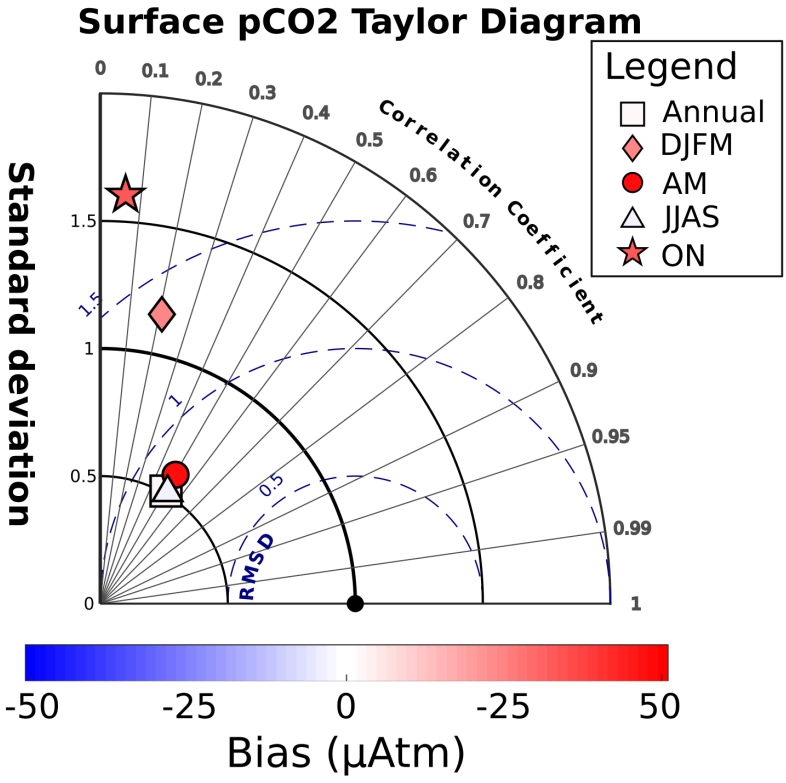

Figure 4. Taylor diagram of modeled vs. observed surface pCO_2, both in total and seasonal sub-sampling. Data are from merged SOCAT and LDEO databases, corrected to year 2005. Distance frmo origin (concentric solid lines) is normalized model standard deviation. Angle from vertical axis is Pearson correlation coefficient. Distance from observation point (black dot) is root-mean square deviation (blue dashed lines). Color of each point denotes model bias, *i.e.* positive values are overestimate.

https://doi.org/10.5194/bg-2021-22
Preprint. Discussion started: 17 February 2021

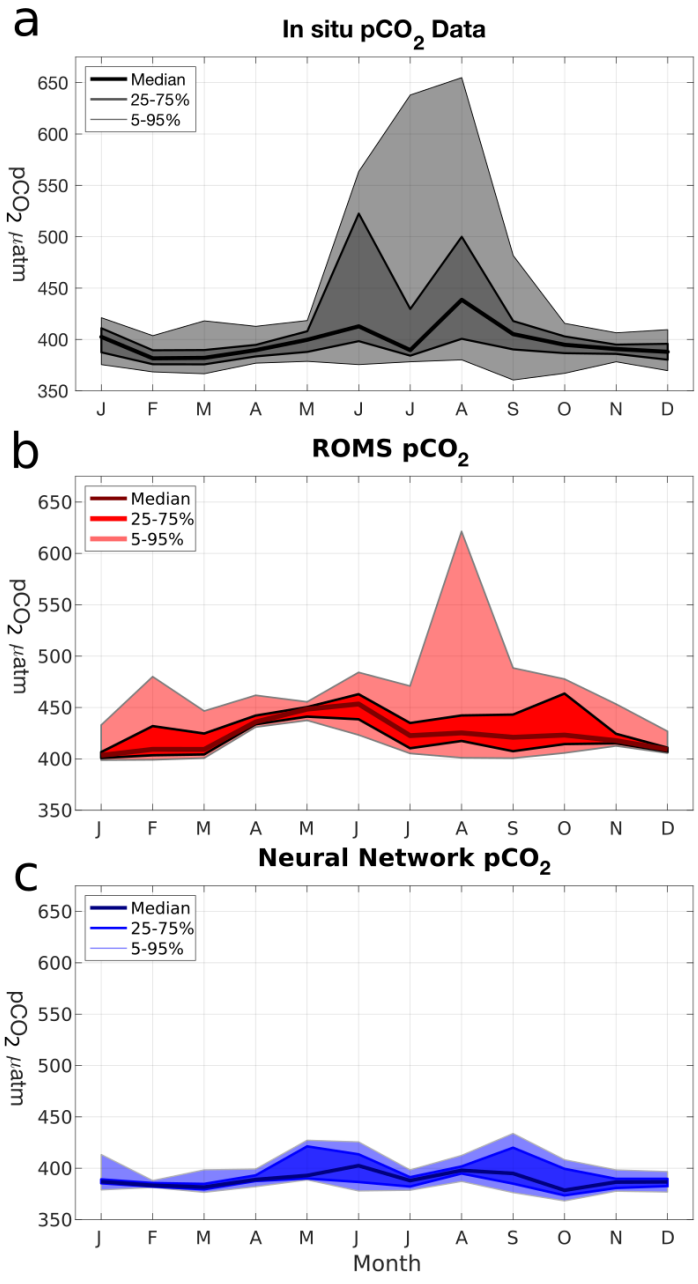

Figure 5. Monthly probability density distributions of surface pCO_2 in (a) merged SOCAT/LDEO *in situ* data, (b) modeled pCO_2, and (c) L15 pCO_2 climatology.

https://doi.org/10.5194/bg-2021-22
Preprint. Discussion started: 17 February 2021

Biogeosciences
Discussions
Open Access
EGU

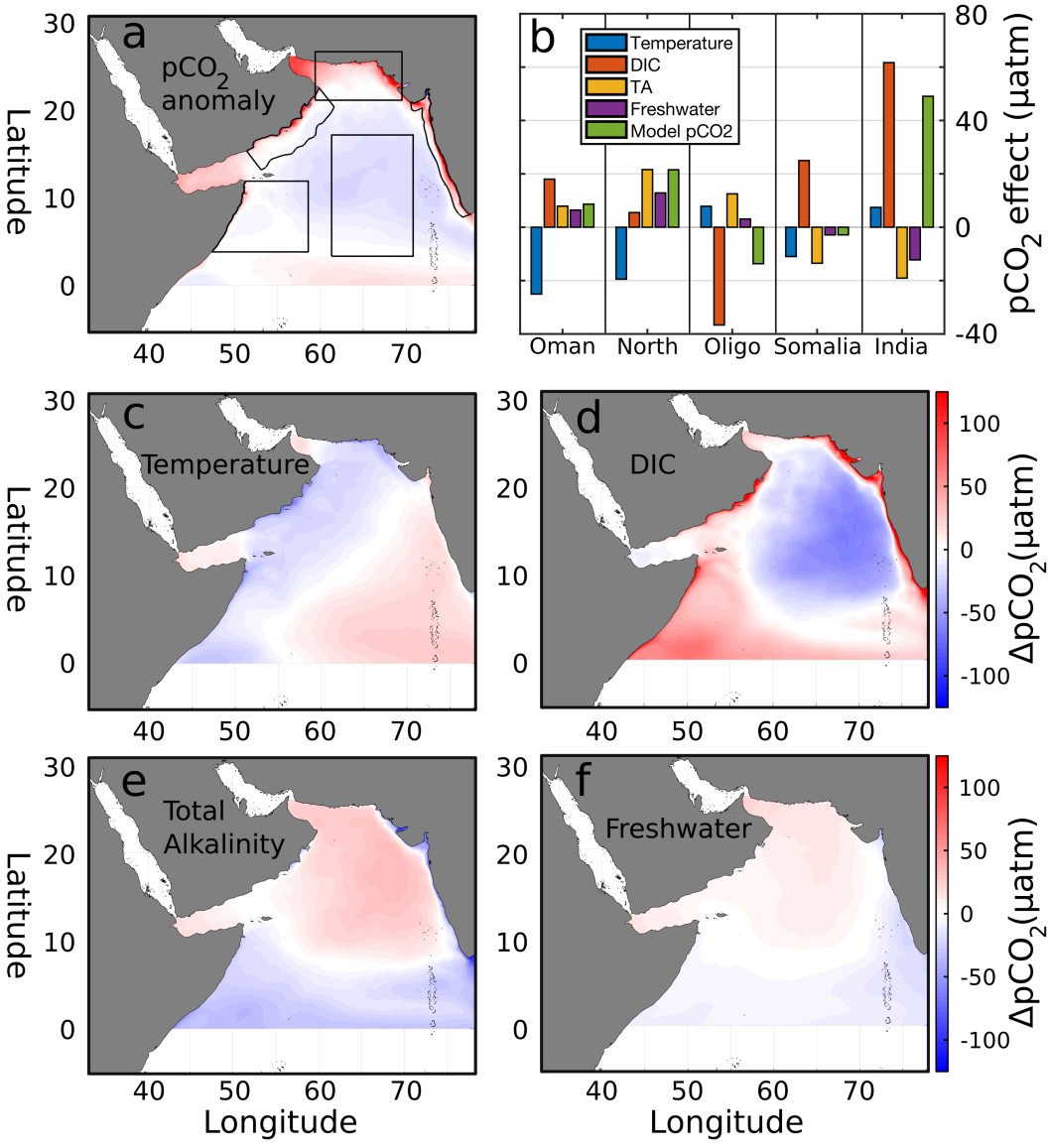

Figure 6. (a) Spatial anomaly of time-averaged surface pCO_2 (μatm). Black boxes represent regions of analysis used in (b) to show averaged contributions of four variables to pCO_2 variability. The changes in pCO_2 due to these variables are shown for (c) temperature, (d) DIC, (e) TA, and (f) freshwater.

https://doi.org/10.5194/bg-2021-22
Preprint. Discussion started: 17 February 2021

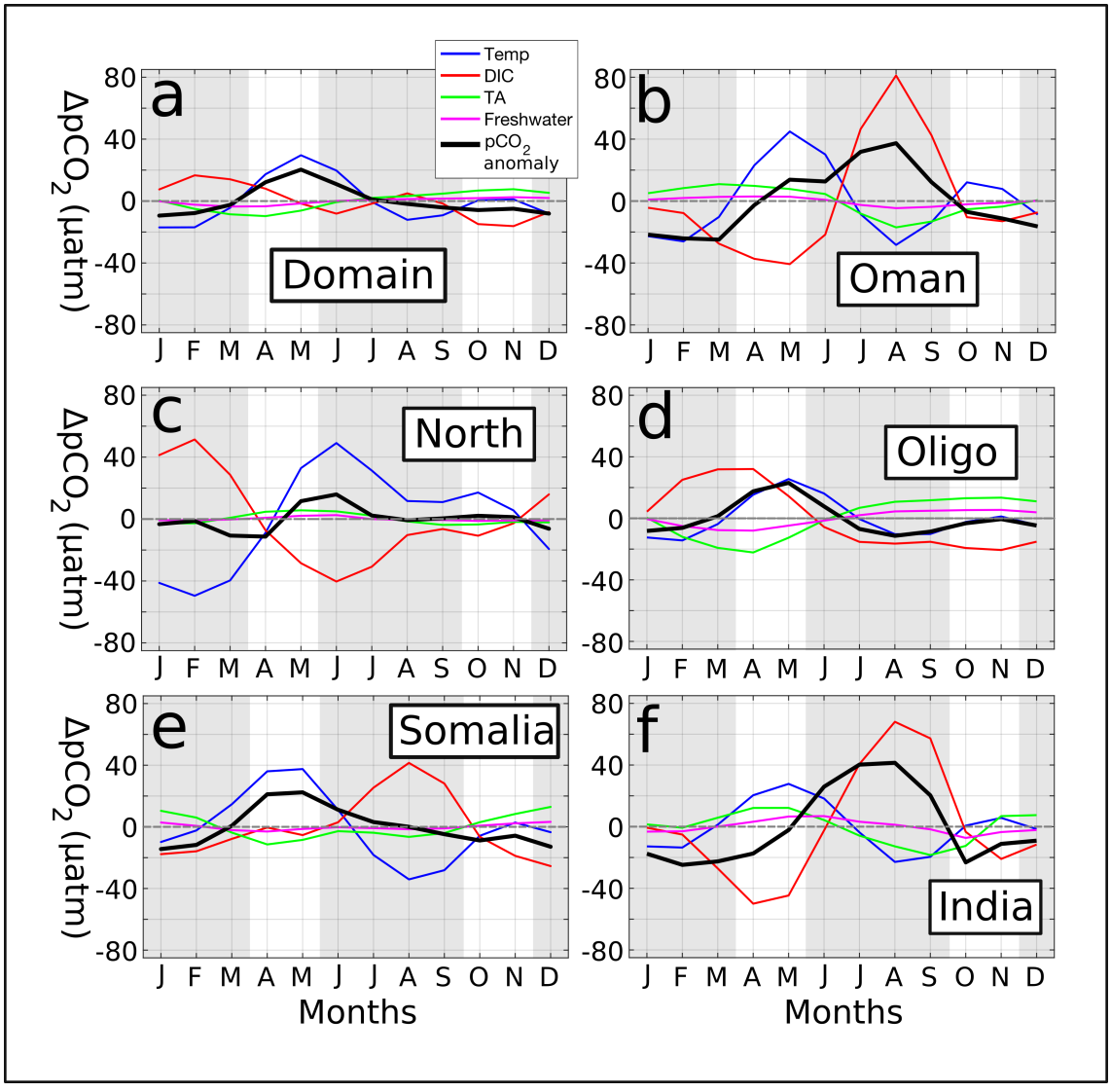

Figure 7. Timeseries of pCO_2 anomalies (μatm) (black lines) for (a) the entire domain, (b) Oman, (c) North AS, (d) oligotrophic central AS, (e) Somalia, and (f) India. Dashed gray lines indicates horizontal axis. Gray shading shows summer and winter monsoons. Additional lines show change in pCO_2 due to temperature (blue), DIC (red), TA (green), and freshwater (magenta).

https://doi.org/10.5194/bg-2021-22
Preprint. Discussion started: 17 February 2021

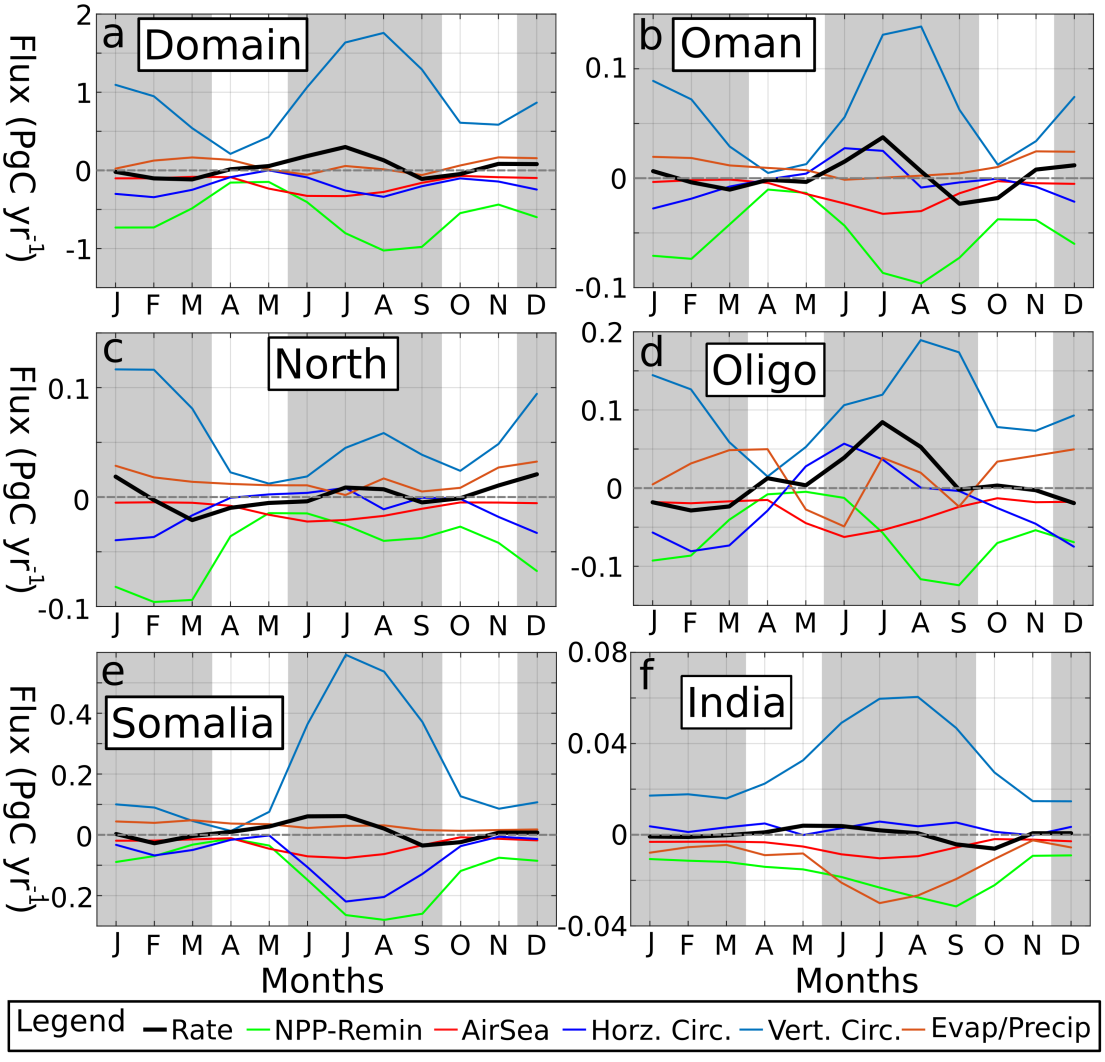

Figure 8. Timeseries of DIC fluxes (PgCyr^{-1}) in the top 20 m for (a) the domain, (b) Oman, (c) North AS, (d) oligotrophic central AS, (e) Somalia, and (f) India. Dashed gray line shows x=zero axis. Gray shading denotes summer and winter monsoons, similar to Fig. 8.

https://doi.org/10.5194/bg-2021-22
Preprint. Discussion started: 17 February 2021

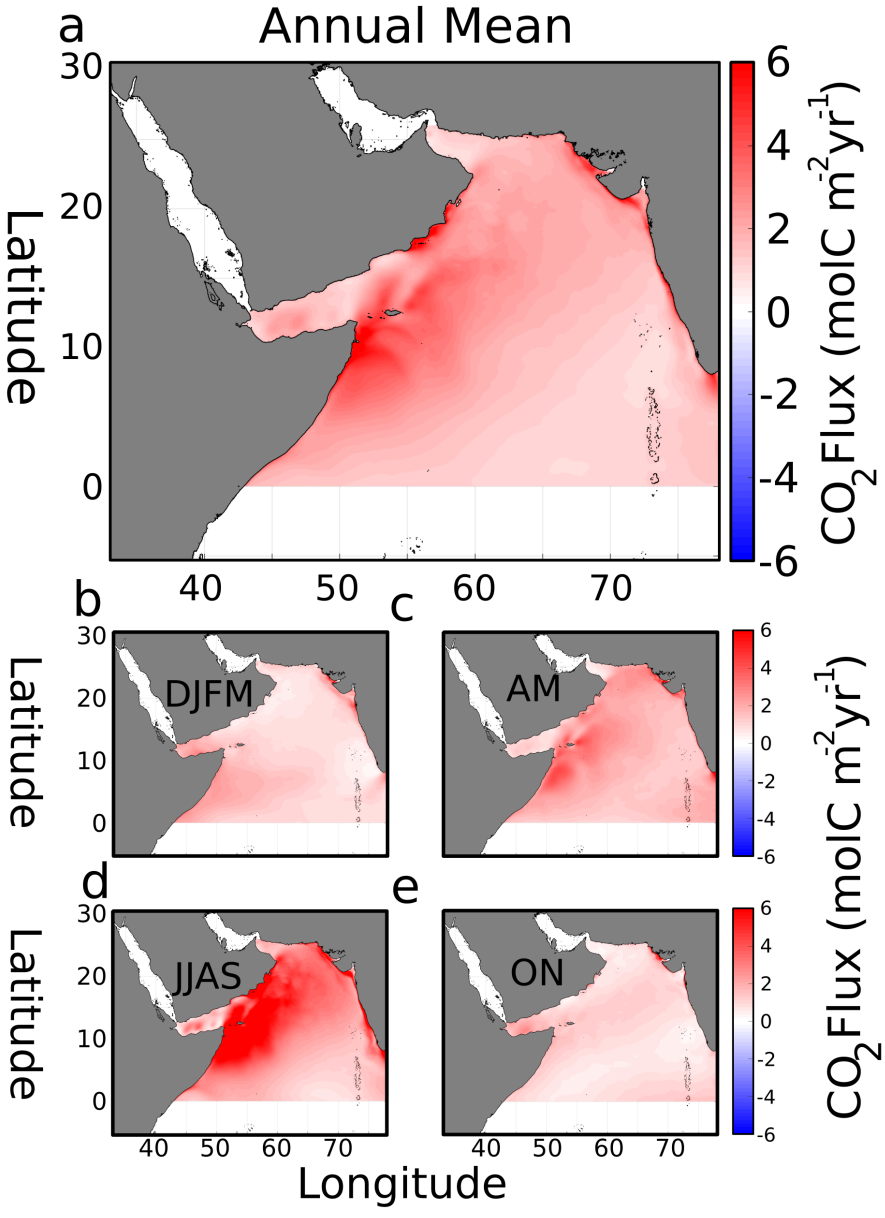

Figure 9. (a) Modeled annual mean air-sea CO_2 flux density ($\mathrm{molC\,m^{-2}yr^{-1}}$). (b-e) Seasonal flux density for winter DJFM, spring AM, summer JJAS, and fall ON, respectively. Positive is flux out of the ocean.

https://doi.org/10.5194/bg-2021-22
Preprint. Discussion started: 17 February 2021

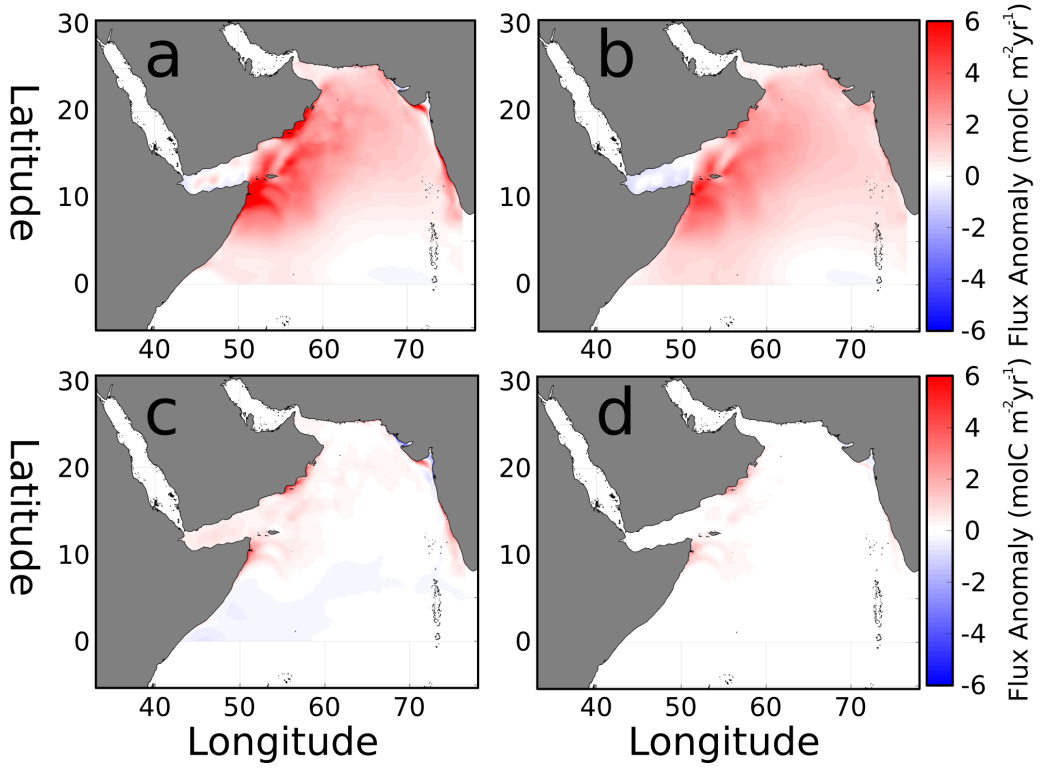

Figure 10. (a) Anomaly of air-sea CO_2 flux during summer monsoon JJAS ($\mathrm{molCm^{-2}yr^{-1}}$. Summer flux anomaly contributions due to (b) wind, (c) pCO_2, and (d) cross-terms in Eqn.(8).

https://doi.org/10.5194/bg-2021-22
Preprint. Discussion started: 17 February 2021

Biogeosciences
Discussions
Open Access
EGU

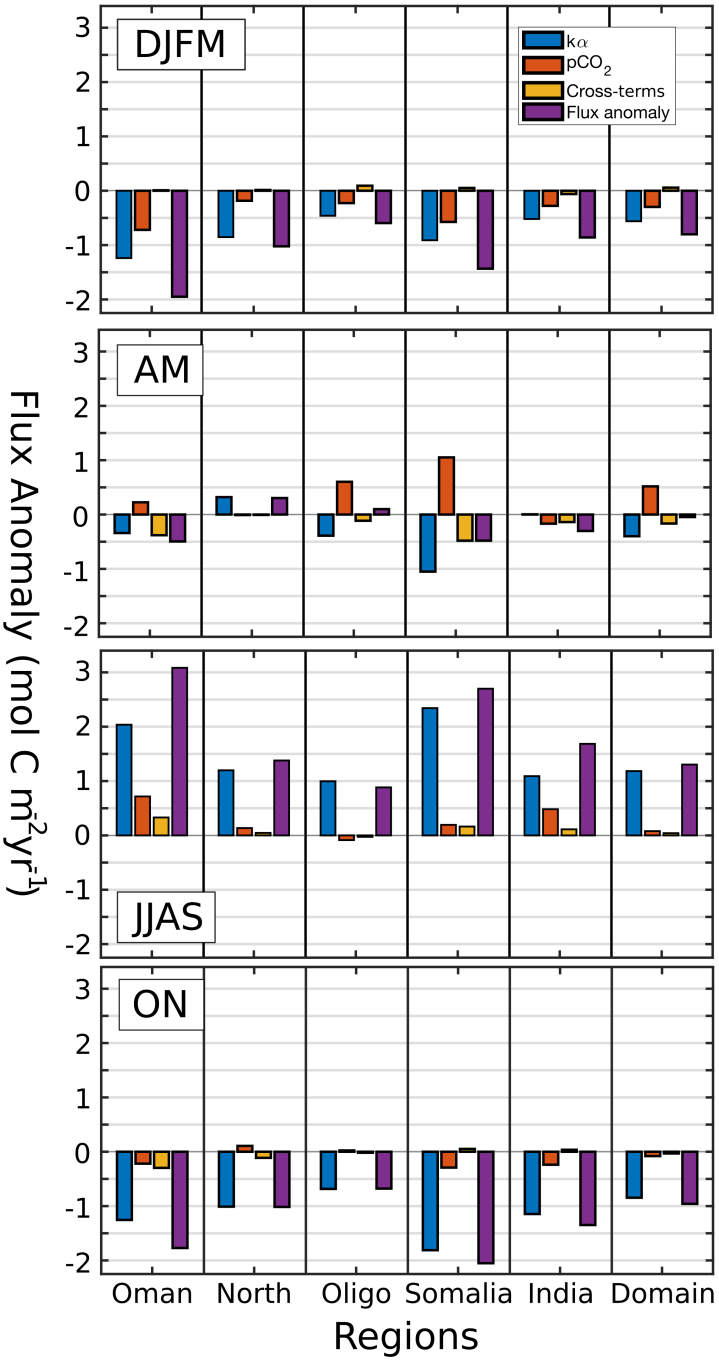

Figure 11. Seasonal CO_2 flux anomaly (purple) for winter DJFM monsoon (top-left), spring AM (top-right), summer monsoon JJAS (bottom-left), and fall ON (bottom-right). Contributors to the flux are solubility/winds ($k\alpha$,blue), pCO_2 (red), and cross-terms (yellow). Results are shown for entire domain and sub-regions.

https://doi.org/10.5194/bg-2021-22
Preprint. Discussion started: 17 February 2021

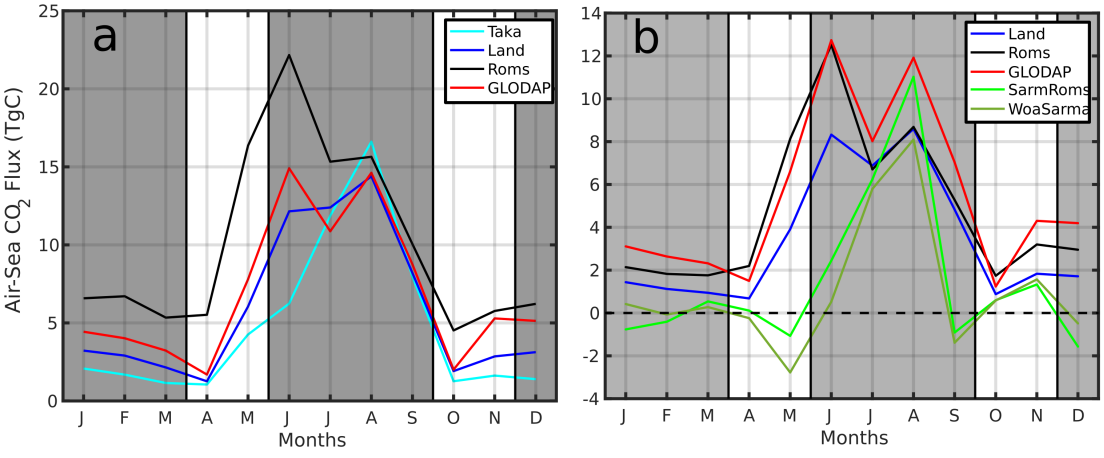

Figure 12. (a) Monthy CO_2 flux (TgC) from the AS as calculated using pCO_2 from TK09 (cyan), L15 (blue), model (black), and GLODAP (red). (b) Monthly CO_2 flux from 10^oN and north using pCO_2 from L15 (blue), model (black), GLODAP (red), Sarma using model output (bright green), and Sarma using WOA data (dark green). Dashed line in (b) is the zero flux axis, gray regions denote winter and summer monsoons. Positive flux is out from the ocean surface.

https://doi.org/10.5194/bg-2021-22
Preprint. Discussion started: 17 February 2021

Biogeosciences
Discussions
Open Access
EGU

Table 1. Summary of pCO_2 datasets used in this study. Included is whether the product is gridded, and if so, its spatial and temporal resolution. Reference year (Ref. Yr) indicates the year from which Keeling atmospheric xCO_2 values are used to calculate CO_2 flux. Purpose designates use case within the article. pCO_2 calculated indicates whether product provides pCO_2 (No) or whether pCO_2 was calculated using DIC, TA, temperature, salinity, and possibly Chl-*a* (Yes).

Dataset	**Gridded (Y/N), Resolution**	**Ref. Year (xCO_2)**	**Domain**	**Purpose**	**pCO_2 calculated**	**Reference**
Surface Ocean Carbon Atlas (SOCAT)	No, N/A	2005	Global	Model pCO_2 validation	No	Bakker et al. (2016)
Lamont-Doherty Earth Observatory pCO_2 database (LDEO)	No, N/A	2005	Global	Model pCO_2 validation	No	Takahashi et al. (2019)
Takahashi 2009 (TK09)	Yes, 4^ox5^o, monthly	2005	Global	Air-Sea CO_2 flux estimate	No	Takahashi et al. (2009)
Landschützer 2015 (L15)	Yes, 1^ox1^o, monthly	2001	Global	pCO_2 comparison and Air-Sea CO_2 flux estimate	No	Landschützer et al. (2015)
Sarma statistical model, T/S/Chl-*a* from model (ROMS)	Yes, $1/24^o$ (interpolated to 1^o), seasonal	1995	AS north of 10^oN	Air-Sea CO_2 flux estimate	Yes	Sarma (2003)
Sarma statistical model, World Ocean Atlas T/S, SeaWifs Chl-*a*	Yes, 1^ox1^o, seasonal	1995	AS north of 10^oN	Air-Sea CO_2 flux estimate	Yes	Sarma (2003)
GLODAP DIC/TA, World Ocean Atlas T/S	Yes, 1^ox1^o, annual	2002	Global	Air-Sea CO_2 flux estimate	Yes	Olsen et al. (2019)